GeoExpert ag

swiss*nuclear*: PEGASOS Refinement Project:
SP2 – Ground Motion Characterization

Contract no. PMT-VT-1032

Seismic Shear Wave Velocity Determination and Hybrid Seismic Survey at the SED-Station WILA (Turbenthal ZH)

Date of Field Data Acquisition 15th April 2009

Revised Report

Client

swiss*nuclear*
Project PRP
Frohburgstrasse 17
4601 Olten

Contractor

GeoExpert ag
Seismic Prospecting
Ifangstrasse 12b
P.O. Box 451
8603 Schwerzenbach

8603 Schwerzenbach, 12th June 2009

INDEX

1 INTRODUCTION

1.1 Survey objectives

The seismic survey's main task is to provide information about the distribution function of the shear wave velocities in the depth interval of the uppermost 30 m along a 100 m long seismic profile.

Additionally, the following objectives are to be met:

- the mapping of the topography of the rock face, i.e. the thickness of the Quaternary deposits;
- the determination of the thickness of the weathered zone and its degree of decompaction at the bedrock surface;
- a general view of geological structures.

1.2 The choice of the appropriate surveying methods

Several methods are available for deriving the s-wave velocity distribution in the subsurface at any given position:

- in-situ measurement by down-hole or crosshole seismic surveying;
- shear-wave refraction tomography profiling;
- dispersion analysis of surface waves (MASW; **M**ultiple channel **A**nalysis of **S**urface **W**aves)

The surveys are to be carried out at, or as close as possible near some 20 SED earth quake monitoring stations in Switzerland. Ideally, the surveys are to be conducted on two orthogonal profiles in order to derive at their point of intersection a robust 1D s-wave velocity distribution function by correlation. To this end, the methods of MASW and shear-wave refraction tomography profiling are to be combined.

The results are to include the following fundamental parameters $v_{s,5}$, $v_{s,10}$, $v_{s,20}$, $v_{s,30}$, $v_{s,40}$, $v_{s,50}$, $v_{s,100}$ are to be calculated, also an error estimation of all values.

The data acquired for the MASW method are to be subjected to complementary **p-wave hybrid seismic data processing** in order to image the geological structures.

2 FIELD DATA ACQUISITION PARTICULARS

2.1 Time Schedule

Date	*Time*	*Activities / remarks*
15.04.2009	1340	arrival from Schwerzenbach
	1340 - 1355	site reconnaissance
	1355 - 1430	lay-out of recording spread profile 1 s- & p-wave
	1445 - 1515	compressional wave data recording profile 1
	1530 - 1610	shear wave data recording profile 1
	1610 - 1740	lay-out of recording spread profile 2 s- & p-wave
	1740 - 1800	compressional wave data recording profile 2
	1815 - 1935	shear wave data recording profile 2
	1940 - 2000	retrieval of the recording spread
	2000	departure from site

2.2 Summary of Data Acquisition Parameters

Compressional Wave Data Acquisition

# of active channels	96
geophone type	4.5 Hz natural frequency, vertical velocimeter
receiver station spacing	1.0 m
# of geophones/station	1
source point spacing	2.0 m to 3.0 m
source type	vertical hammer (6 kg) striking on a horizontal metal plate
sampling rate	500 µs
recording time	2048 ms
field filters	0.5 Hz LC, anti-alias
# of field records	49 (line 09SN_19WILA-P1) and 49 (line 09SN_19WILA-P2)

Shear Wave Data Acquisition

# of active channels	48
geophone type	10 Hz natural frequency, horizontal velocimeter
receiver station spacing	2.0 m
# of geophones/station	1
source point spacing	4.0 m to 6.0 m
source type	horizontal hammer (6 kg) striking horizontally at a metal-plated wooden beam anchored to the ground by means of 20 cm long spikes
sampling rate	500 µs
recording time	512 ms
field filters	2 Hz LC, anti-alias
# of field records	50 at 25 positions on both lines

Fig. 2.1: S-wave data acquisition at profile 09SN_19WILA-S1.

2.3 Composition of Seismic Field Crew

Personnel

Lorenz Keller	Dipl. Natw. ETHZ, Geophysicist, party chief
Jochen Fiseli	Dipl.-Geolog, University of Freiburg I. Br., assistant
Mischa Froidevaux	Dipl. Natw. ETHZ, Geophysicist, assistant

Equipment

96	vertical geophones 4.5 Hz
48	horizontal geophones 12 Hz
6	seismic cables
1	seismic acquisition system Summit Compact, 96 channels
1	laptop computer for data acquisition
3	walkie-talkies
1	hammer 6 kg
1	steel plate
1	metal-plated wooden beam
1	off-roader (Nissan Patrol 4x4)

2.4 Location

The seismic monitoring station WILA (Turbenthal ZH) is situated on the top of a Tertiary sediment ridge in northeastern Switzerland, canton of Zurich. The sediments are bad sorted conglomerates (Nagelfluh) of the Hörnli alluvial fan (Upper Freshwater Molasse).

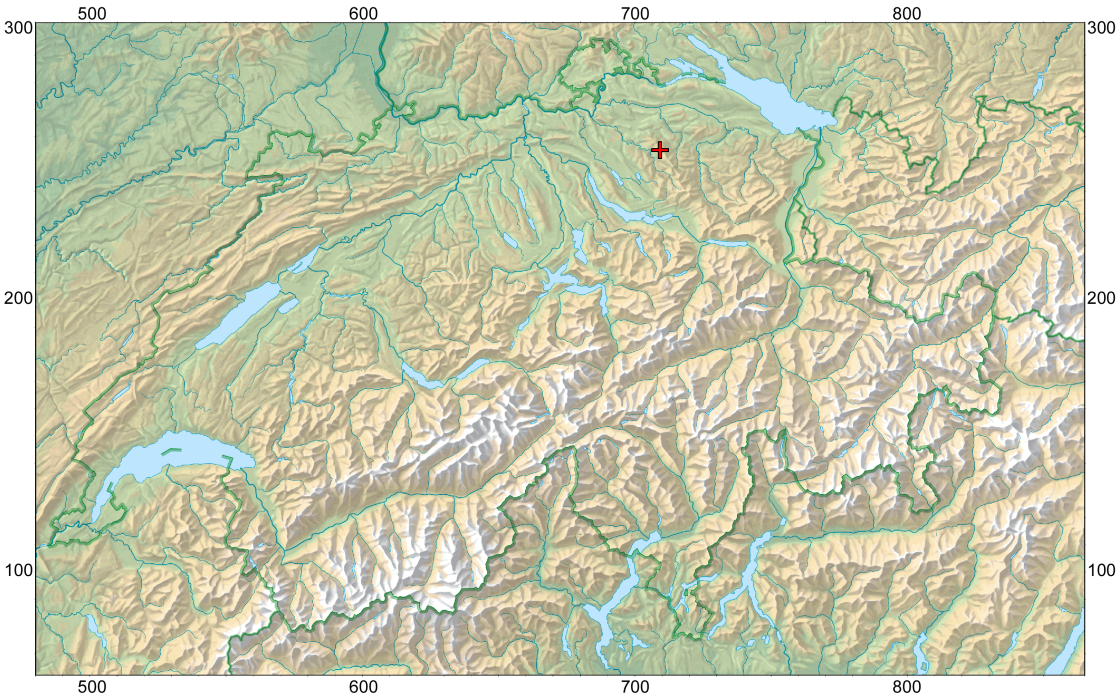

Fig. 2.2: The red cross marked seismic monitoring station WILA (Turbenthal ZH) is located in Zurich's Tertiary sediments (Upper Freshwater Molasse). (map: geodata @ swisstopo).

2.5 Recording Conditions and Line Setup

Sunny and warm weather prevailed throughout the field data recording period. No external noise sources could be observed.

In general, the seismic data quality obtained at WILA is to be rated as high, also is the dispersion content of surface waves.

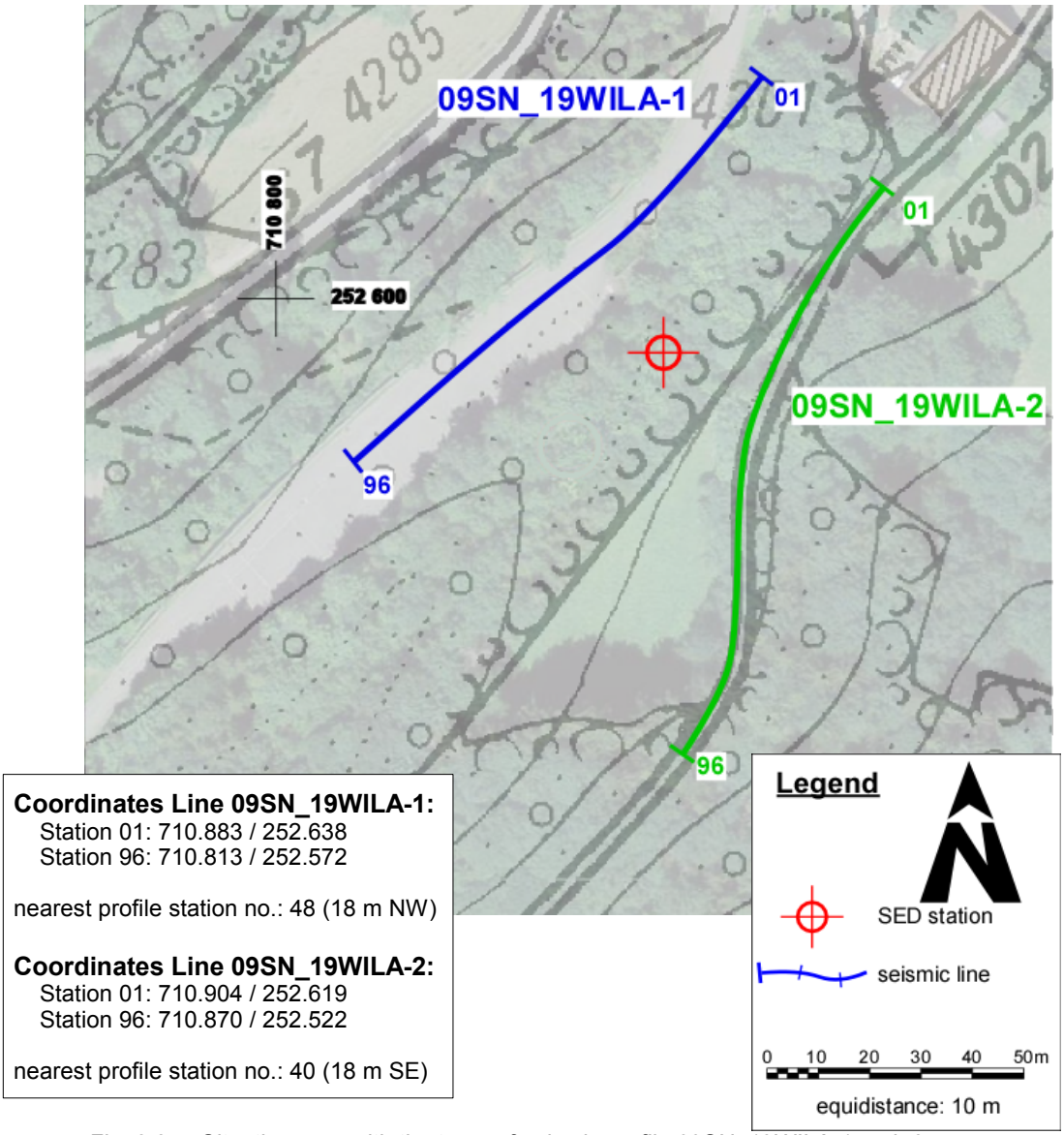

Coordinates Line 09SN_19WILA-1:
Station 01: 710.883 / 252.638
Station 96: 710.813 / 252.572

nearest profile station no.: 48 (18 m NW)

Coordinates Line 09SN_19WILA-2:
Station 01: 710.904 / 252.619
Station 96: 710.870 / 252.522

nearest profile station no.: 40 (18 m SE)

Fig. 2.3: Situation map with the trace of seismic profile 09SN_19WILA-1 and -2. (background map: © GIS-ZH / ARV canton of Zurich.)

3 SEISMIC DATA PROCESSING AND IMAGING OF THE RESULTS

3.1 General Remarks

- For the shear and compressional wave refraction seismic evaluation the package **RAYFRACT** by Intelligent Resources Ltd., Vancouver CAN, was used. The system features the technique of diving wave tomography (www.rayfract.com).
- The system **SPW** (**S**eismic **P**rocessing **W**orkshop) of Parallel Geoscience Corporation, Austin US-TX, was used for reflection seismic data processing (www.parallelgeo.com).
- Data processing of surface waves (MASW processing) was conducted with the software package **SurfSeis** V2.0 of Kansas Geological Survey in Lawrence US-KS.

A detailed description of the various surveying methods will be included in the general summary report.

3.2 Shear Wave Refraction Tomography

3.2.1 Reformatting and field geometry assignment

After reformatting the field data into the Rayfract format the field geometry is applied.

3.2.2 First break time picking

At each shot position, two seismic records were acquired in both activation directions. These two records are displayed superimposed with different colors on each other in Fig 3.2a together with the manually determined first arrival time picks.

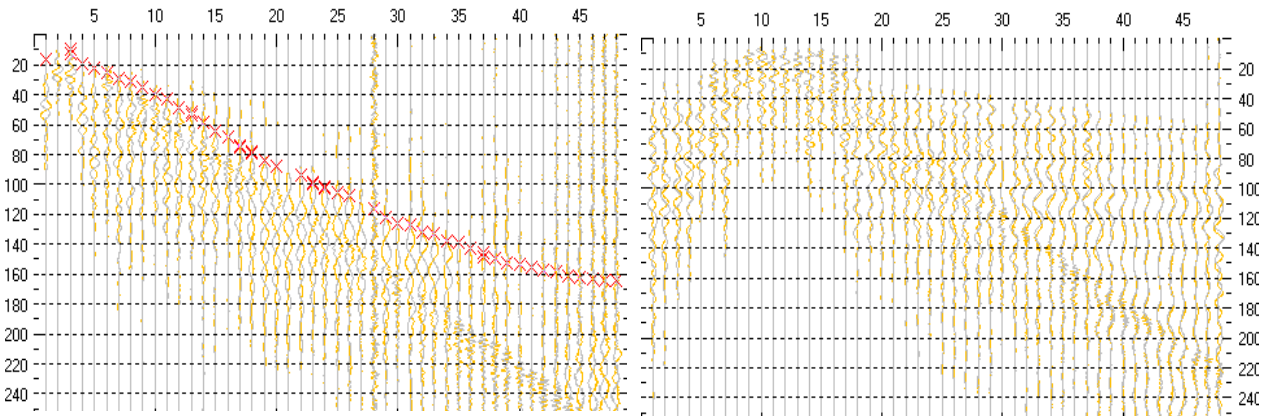

Fig. 3.2a: Comparison of two records of seismic shear wave profile 09SN_19WILA-S1, one (left) on soft soil with normal bonding between source and soil and the other one (right) on asphalt seal without any hint of shear wave arrivals. Nevertheless, the dataset was processed completely but without sufficient true shear wave velocity determination.

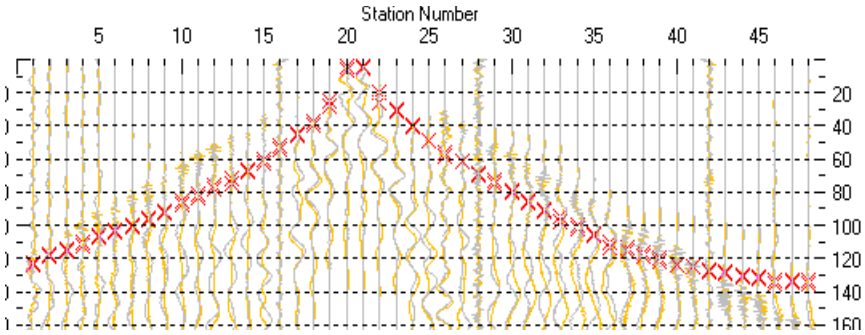

Fig. 3.2b: Moderate quality dual field record of line 09SN_19WILA-S2showing at each station the s-wave traces with opposing polarities in different colors. The manually picked s-wave refraction arrivals at each station are marked with an x. The station spacing is 2 m, profile station number 00 = profile meter 0; profile station number 48 = profile meter 96.

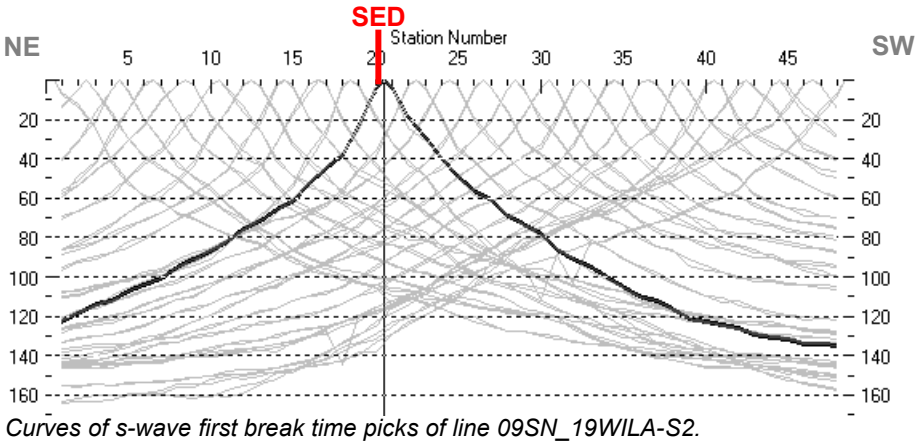

Fig. 3.2c: Curves of s-wave first break time picks of line 09SN_19WILA-S2.

3.2.3 Analytical Determination of Refraction Velocities

An initial 1D-velocity function (averaged 1D velocity-depth profiles derived by the Delta-t-V method, see Tab. 3.2a) is determined in the 3-dimensional time-offset-CMP-domain of all first break arrival time curves in the 3-dimensional time-offset-CMP-domain (see. Fig. 3.2d).

Depth [m]	Vs [m/s]
0.0	1627
0.3	1510
0.7	1289
1.0	1130
1.4	1040
2.1	970
2.8	994
3.8	1111
5.2	1278
6.8	1408
9.1	1600
12.0	1907
15.7	2042
20.6	2331
26.8	2433
35.2	3392

Depth [m]	Vs [m/s]
0.0	261
0.4	258
0.7	251
1.1	244
1.4	239
2.1	241
2.8	253
3.9	275
5.3	353
6.9	478
9.2	544
12.2	520
16.0	693
20.9	837
27.3	1013
35.8	1326
46.7	1972

Tab. 3.2a: Initial 1D s-wave velocity function derived from real data of both lines 09SN_19WILA-S1 (left) and -S2 (right). The mean values between profile meters 40 and 50 are shown.

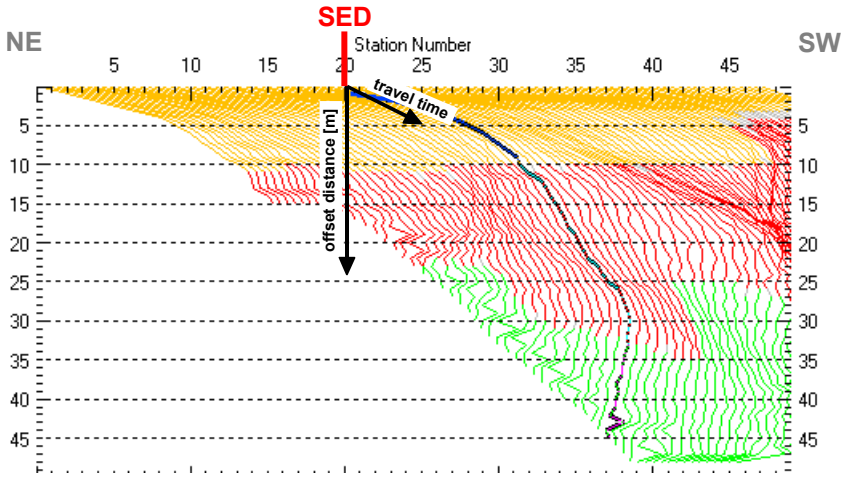

Fig. 3.2d: 3-dimensional distance-travel time diagrams of line 09SN_19WILA-S2 at the mid-points between source points and receiver stations are instrumental when using the analytical CMP derivation of the initial velocity field.
The horizontal axes are the along the CMP positions and the travel time respectively, the vertical axis denotes the offset distance between source and receiver positions. The colors represent different velocity layers. The station spacing is 2 m, profile station number 00 = profile meter 0; profile station number 48 = profile meter 96. The colors represent different velocity layers.

3.2.4 Tomographic inversion of the velocity gradient field by iterative modeling

The velocity field is iteratively refined by the subsequent Wavepath Eikonal Traveltime (WET) tomographic inversion process. The inversion results are portrayed in Fig. 3.2e as a gridded velocity contour section and in Fig. 3.2f as a ray path density section.

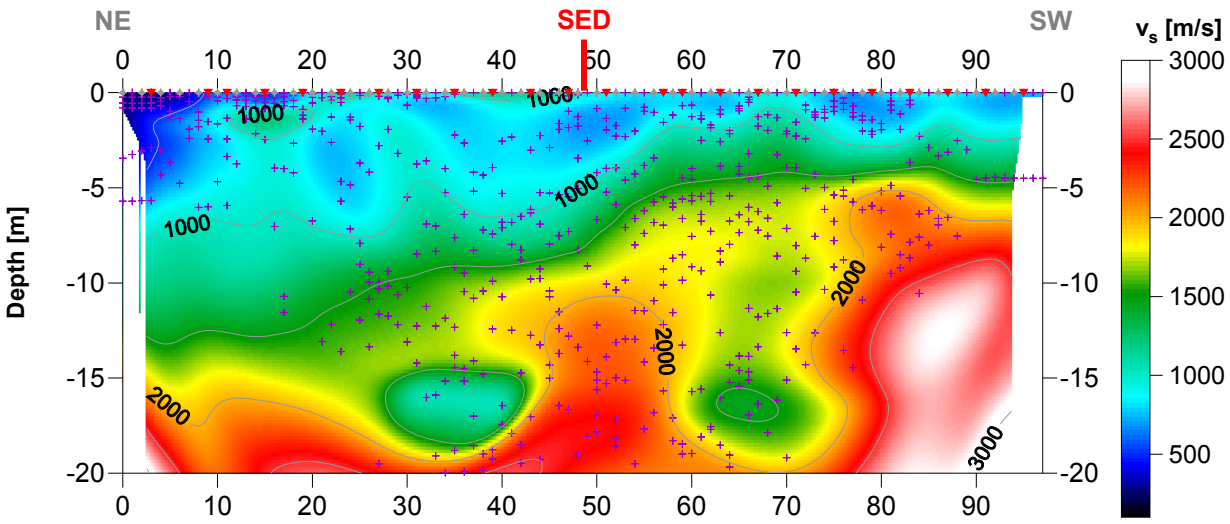

Fig. 3.2e: Shear wave velocity field of the line 09SN_19WILA-S1. Red/white colors denote solid rock, blue/black colors point to unconsolidated sediments and soil.
Vertical axis: depth below terrain [m]; horizontal axis: profile meter; color encoded scale: v_S [m/s]; vertical exaggeration: 2:1; gray diamonds: receiver positions; red triangles: source positions; magenta crosses: positions of determined velocity values. The station spacing is 2 m, profile meter 0 = profile station number 00, profile meter 96 = profile station number 48.

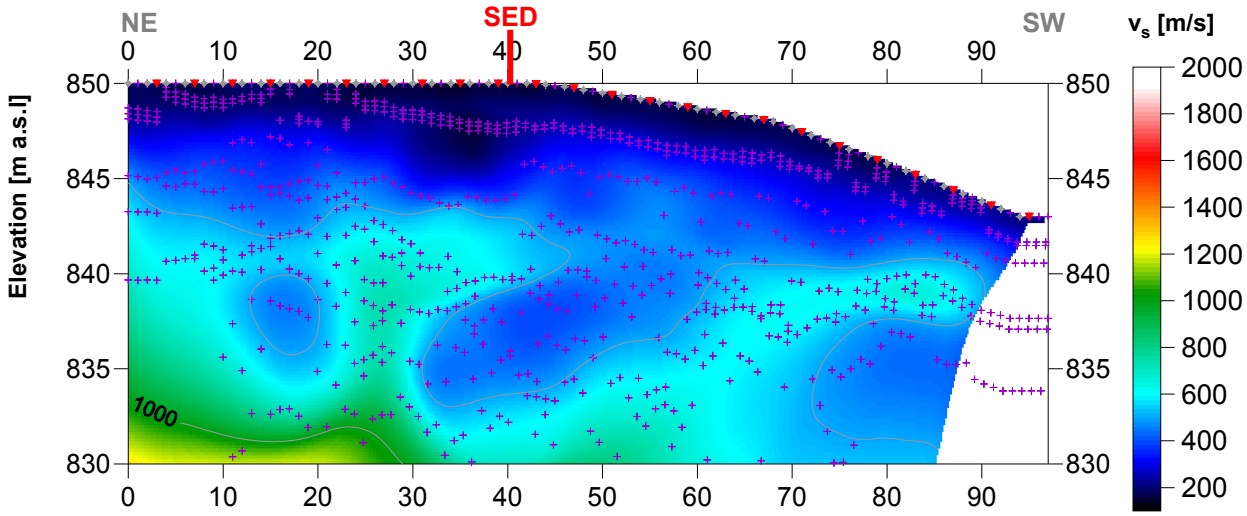

Fig. 3.2f: Shear wave velocity field of the line 09SN_19WILA-S2. Red/white colors denote solid rock, blue/black colors point to unconsolidated sediments and soil.
Vertical axis: elevation [m a.s.l]; horizontal axis: profile meter; color encoded scale: v_s [m/s]; vertical exaggeration: 2:1; gray diamonds: receiver positions; red triangles: source positions; magenta crosses: positions of determined velocity values. The station spacing is 2 m, profile meter 0 = profile station number 00, profile meter 96 = profile station number 48.

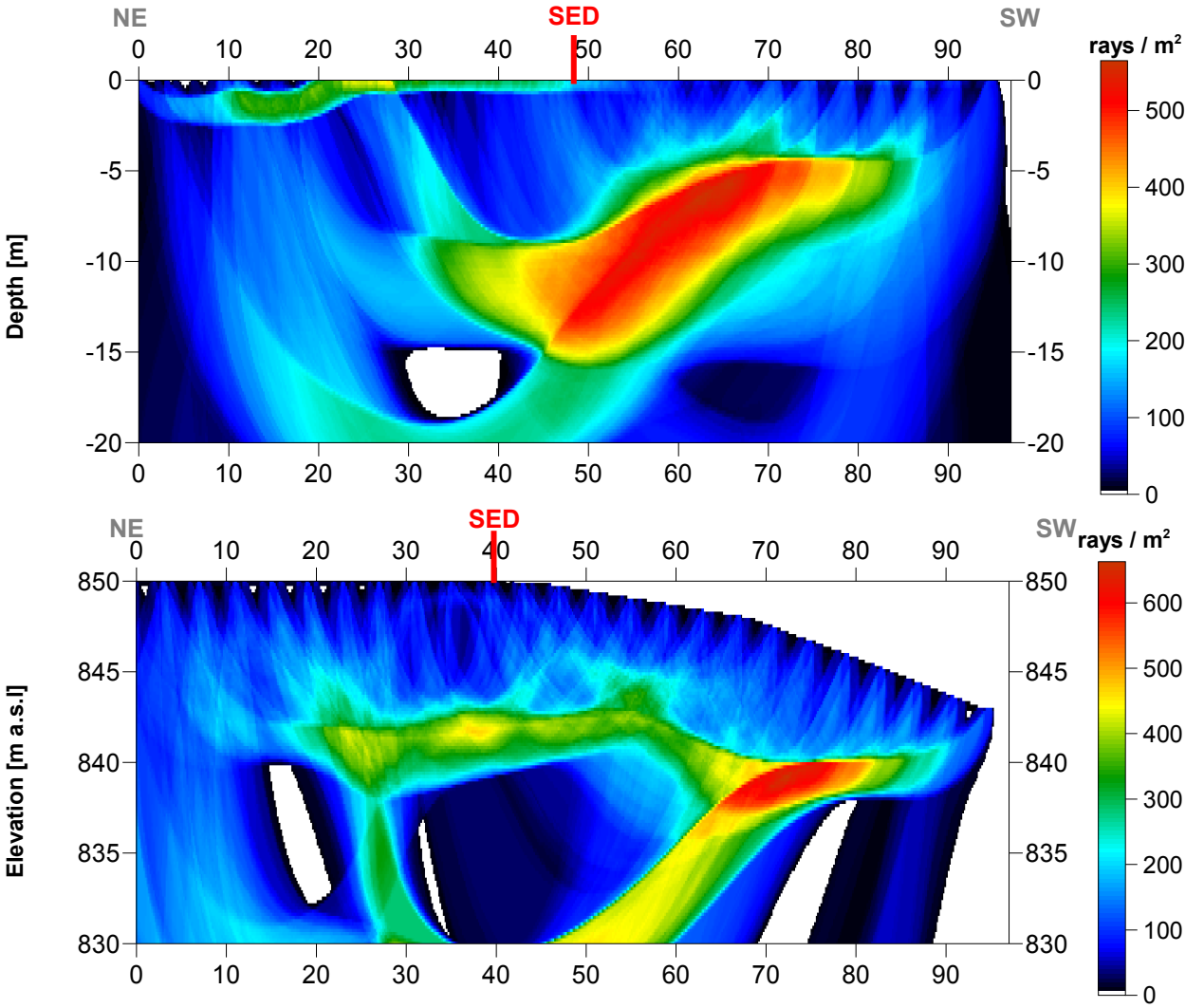

Fig. 3.2g: Shear wave ray path density along the seismic line 09SN_19WILA-S1 (top) and -S2 (bottom). Red/white colors indicate high velocity contrasts (usually at the bedrock surface), blue/black colors denote low coverage areas.

Depth [m]	Vs [m/s]
0.0	931
2.4	863
4.9	1162
7.3	1477
9.8	1842
12.2	2046
14.6	2008
16.9	2209
19.3	2315
21.8	2070
24.2	1880
26.7	2172
29.1	2492
31.5	2720
33.8	2969
36.3	3160
38.7	3289

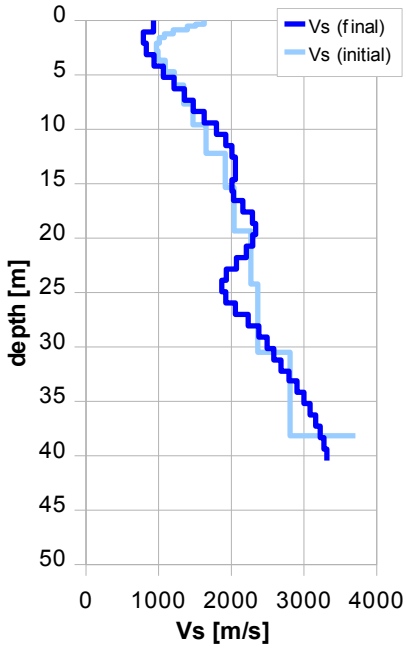

Tab. 3.2b: Final 1D s-wave velocity model derived from real data of line 09SN_19WILA-S1 (horizontal average of all values) for the profile segment (between profile meters 40 and 60) with a geological setting resembling the one at the SED station. The calculated values of the initial 1D s-wave velocity model are given in Tab. 3.2a.

Depth [m]	Vs [m/s]
0.0	163
1.8	246
3.5	345
5.3	411
7.1	472
8.9	485
10.6	452
12.4	454
14.2	514
16.0	589
17.6	670
19.3	751
21.1	852
22.9	879
24.7	881
26.4	927
28.2	989

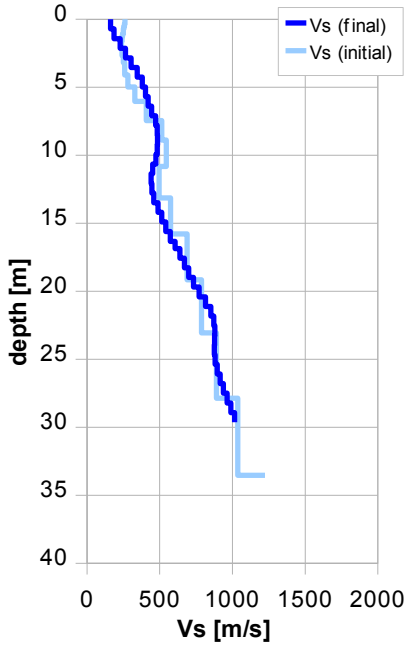

Tab. 3.2c: Final 1D s-wave velocity model derived from real data of line 09SN_19WILA-S2 (horizontal average of all values) for the profile segment (between profile meters 40 and 60) with a geological setting resembling the one at the SED station. The calculated values of the initial 1D s-wave velocity model are given in Tab. 3.2a.

3.3 MASW Processing

3.3.1 Reformatting and field geometry assignment

The data preparation steps for the dispersion analysis include

- the assignment of the field acquisition geometry
- the selection of suitable offset ranges (=arrays) between 10 m and 50 m for dispersion, and the splitting of the field records in forward and reverse shooting direction data sets
- the reformatting of the data into the specific KGS format

X - - ... - - o-o-o-...-o-o-o (forward shooting or so-called PLUS direction)
respectively
o-o-o-...-o-o-o - - ... - - X (reverse shooting or so-called MINUS direction).

where **X** = shot position
o = receiver station
- = 1.0 m offset

The active array used at SED-station WILA are the receiver station in the shot offset range between 10 and 50 m.

3.3.2 Calculating the dispersion image (overtone)

The result of dispersion analysis is the color encoded acoustic energy distribution in the phase velocity - frequency plane (see Fig. 3.3a and b).

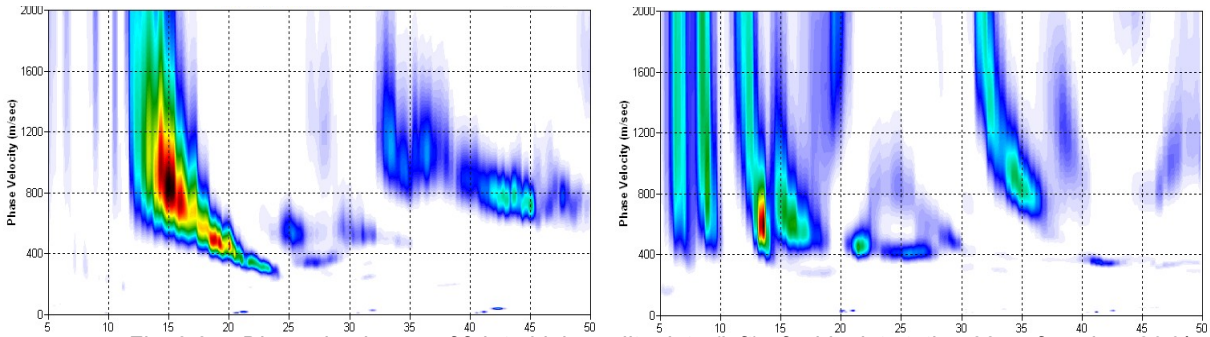

Fig. 3.3a: Dispersion image of fair to high quality data (left) of midpoint station 33 as found on 80 % and of deficient quality data (right) of midpoint station 62 representing about 20 % of the MASW dataset of site WILA.
Horizontal axis: frequency from 5 to 50 Hz; vertical axis: phase velocity from 0 to 2000 m/s; color code: colors from white (no energy) to blue - green - yellow - red - black point to increasing energy amplitude values.

3.3.3 Analysis of the dispersion image

In the dispersion graphs as calculated in section 3.3.2 above, the curves joining the amplitude peaks of the fundamental modes are determined either by subjective inspection or in a semi-automated manner. On datasets with poorly defined amplitude peaks or with a highly irregular alignment of the peaks, the danger of obtaining improbable or wrong results is real and can only be mitigated by the processing experience and the a-priori knowledge of the geological setting by the geophysicist responsible for the data evaluation.

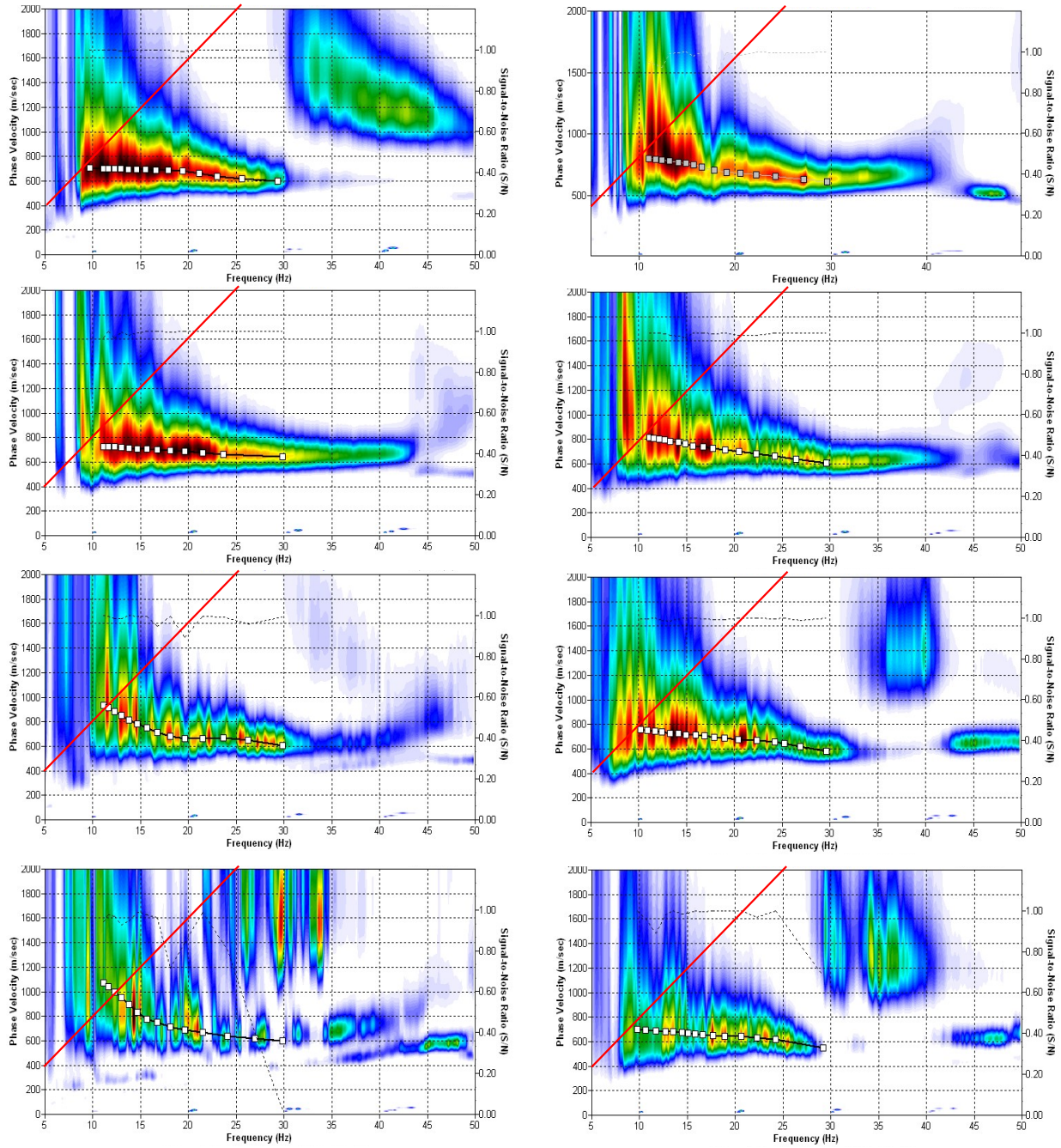

Fig. 3.3b: The manually picked dispersion images used for the derivation of the shear wave velocity section on line 09SN_19WILA-M1. The dispersion curves (squares) are determined by linking the peaks of high energy. Note that 'higher modes' may at times produce higher energy peaks than the fundamental mode required for the analysis.
dotted fine line: signal-noise ratio for the designated f-v_{ph} – value.
red line: high resolution beam-forming curve for v_{max}.
1st row: left: station 41 @ PLUS direction; right: station 42 @ MINUS direction
2nd row: left: station 48 @ PLUS direction; right: station 48 @ MINUS direction
3rd row: left: station 54 @ PLUS direction; right: station 54 @ MINUS direction
4th row: left: station 60 @ PLUS direction; right: station 60 @ MINUS direction

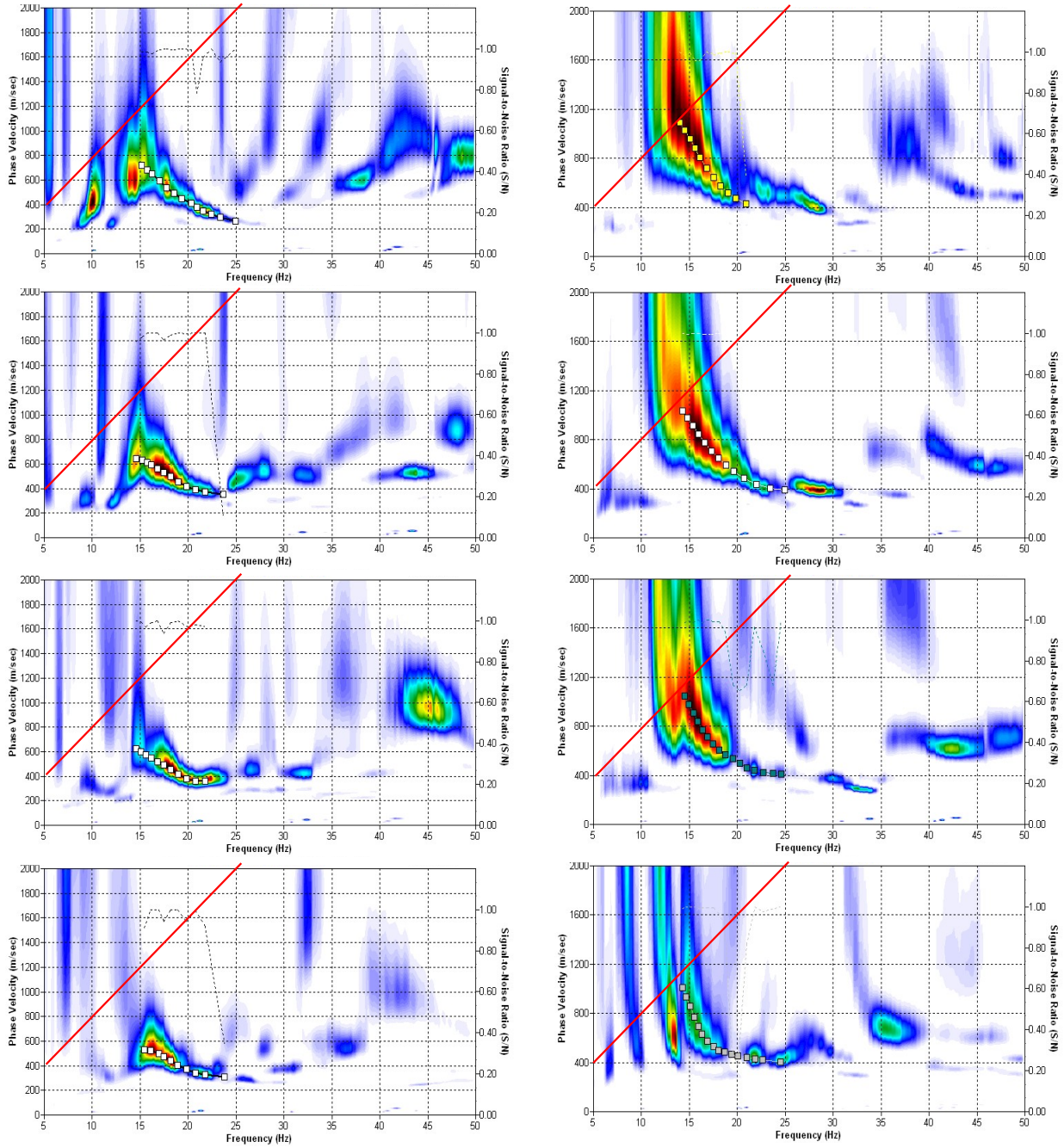

Fig. 3.3c: The manually picked dispersion images used for the derivation of the shear wave velocity section on line 09SN_19WILA-M2. The dispersion curves (squares) are determined by linking the peaks of high energy. Note that 'higher modes' may at times produce higher energy peaks than the fundamental mode required for the analysis.
dotted fine line: signal-noise ratio for the designated f-v_{ph} – value.
red line: high resolution beam-forming curve for v_{max}.
1st row: left: station 41 @ PLUS direction; right: station 42 @ MINUS direction
2nd row: left: station 47 @ PLUS direction; right: station 48 @ MINUS direction
3rd row: left: station 53 @ PLUS direction; right: station 54 @ MINUS direction
4th row: left: station 59 @ PLUS direction; right: station 60 @ MINUS direction

3.3.4 Inversion of dispersion curves resulting in a 1D shear wave velocity distribution

Inversion of the extracted dispersion curves was performed using the algorithm described by Xia et al. (1999).

The inversion process is started by setting the maximum depth (z_{max}) to be in the order of 30% of the largest wavelength for an initial model consisting of 10 layers of increasing thicknesses. For all 10 layers the Poisson's ratio is assumed to be 0.4 and the rock/soil density to be 2.0 g/cm^3. The inversion process is concluded either after twelve iterations or when the convergence condition of a RMS-error of less than 3 m/s (phase velocity) is met.

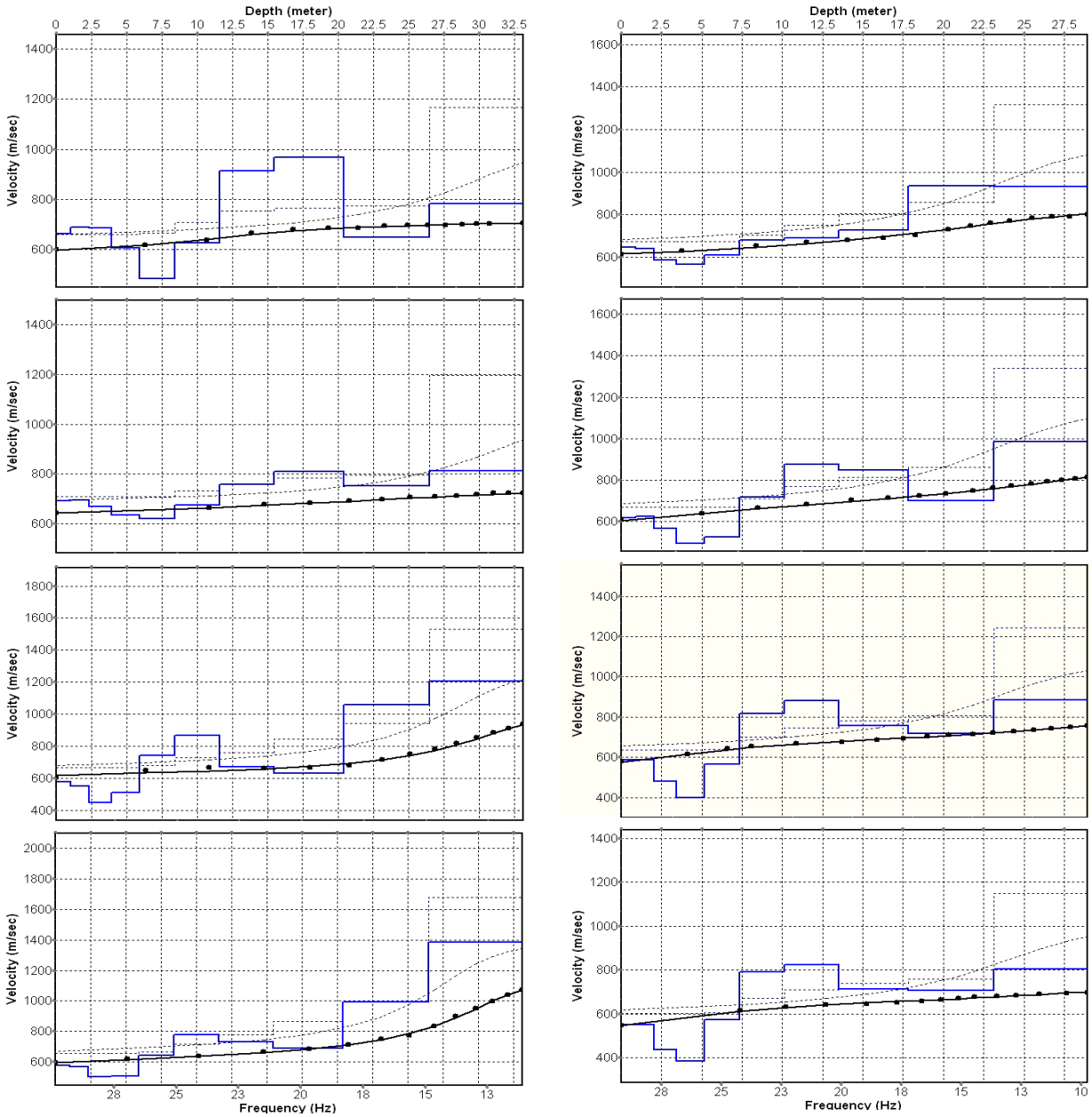

Fig. 3.3d: Inversion results of dispersion curves of dataset at line 09SN_19WILA-M1.
***brown**: Inversion of dispersion curve (dots) resp. of the modeled dispersion curve (dotted line: initial model; continuous line: end model). Horizontal axis: frequency Hz, vertical axis: v_s.*
***blue**: 10-layer-model (dotted: initial model, continuous line: final model). Horizontal axis: depth, vertical axis: phase velocity resp. v_s).*
1st row: left: station 41 @ PLUS direction; right: station 42 @ MINUS direction
2nd row: left: station 48 @ PLUS direction; right: station 48 @ MINUS direction
3rd row: left: station 54 @ PLUS direction; right: station 54 @ MINUS direction
4th row: left: station 60 @ PLUS direction; right: station 60 @ MINUS direction

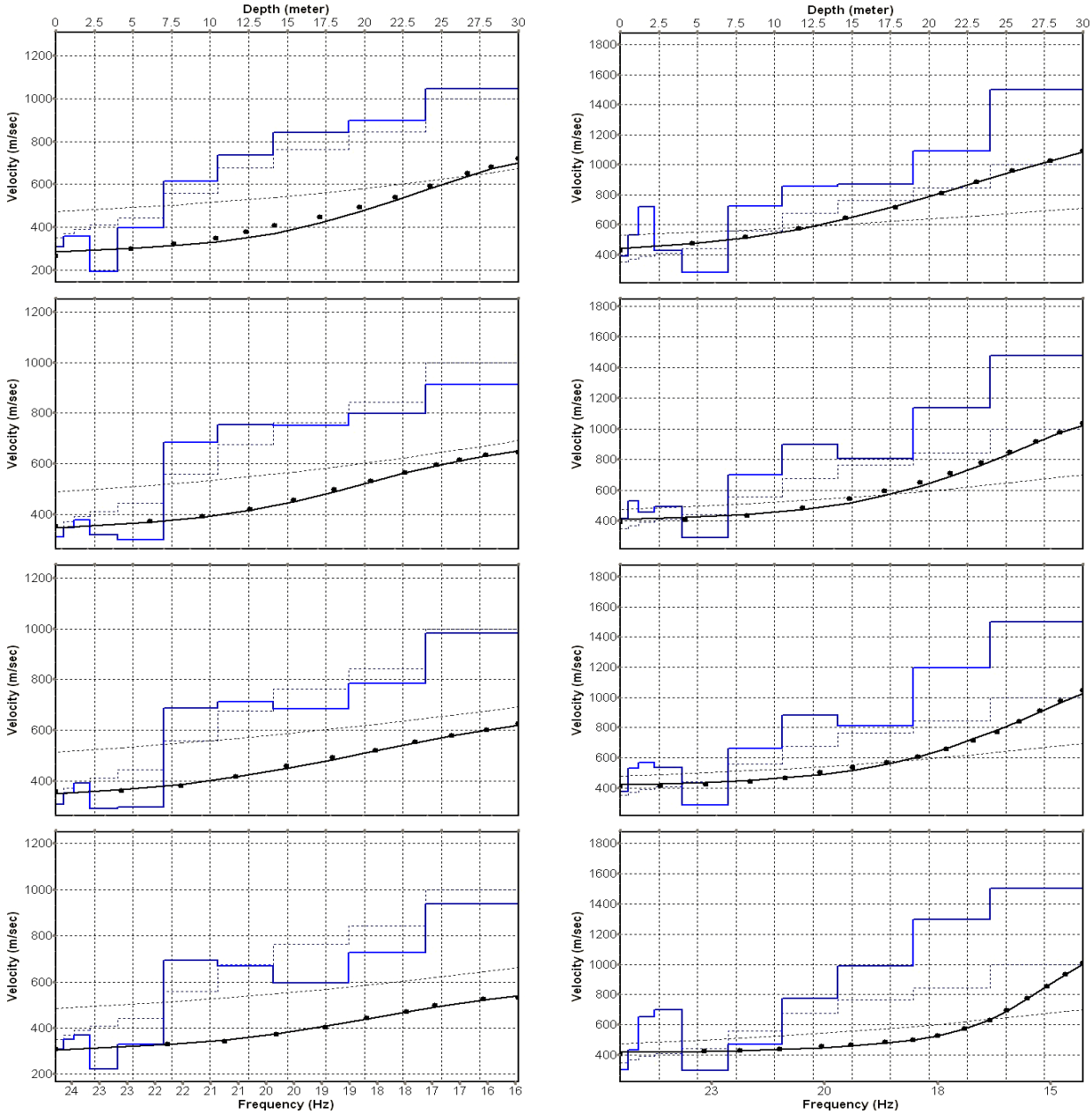

Fig. 3.3e: Inversion results of dispersion curves of dataset at line 09SN_19WILA-M2.
***brown**: Inversion of dispersion curve (dots) resp. of the modeled dispersion curve (dotted line: initial model; continuous line: end model). Horizontal axis: frequency Hz, vertical axis: v_s.*
***blue**: 10-layer-model (dotted: initial model, continuous line: final model). Horizontal axis: depth, vertical axis: phase velocity resp. v_S).*
1st row: left: station 41 @ PLUS direction; right: station 42 @ MINUS direction
2nd row: left: station 47 @ PLUS direction; right: station 48 @ MINUS direction
3rd row: left: station 53 @ PLUS direction; right: station 54 @ MINUS direction
4th row: left: station 59 @ PLUS direction; right: station 60 @ MINUS direction

Dispersion analyses of records with longer receiver arrays should – by theory – increase the investigation depth. At WILA, with both lines and both directions, MASW processing with the maximal array length of 96 m doesn't improve the results (Fig. 3.3f and 3.3g).

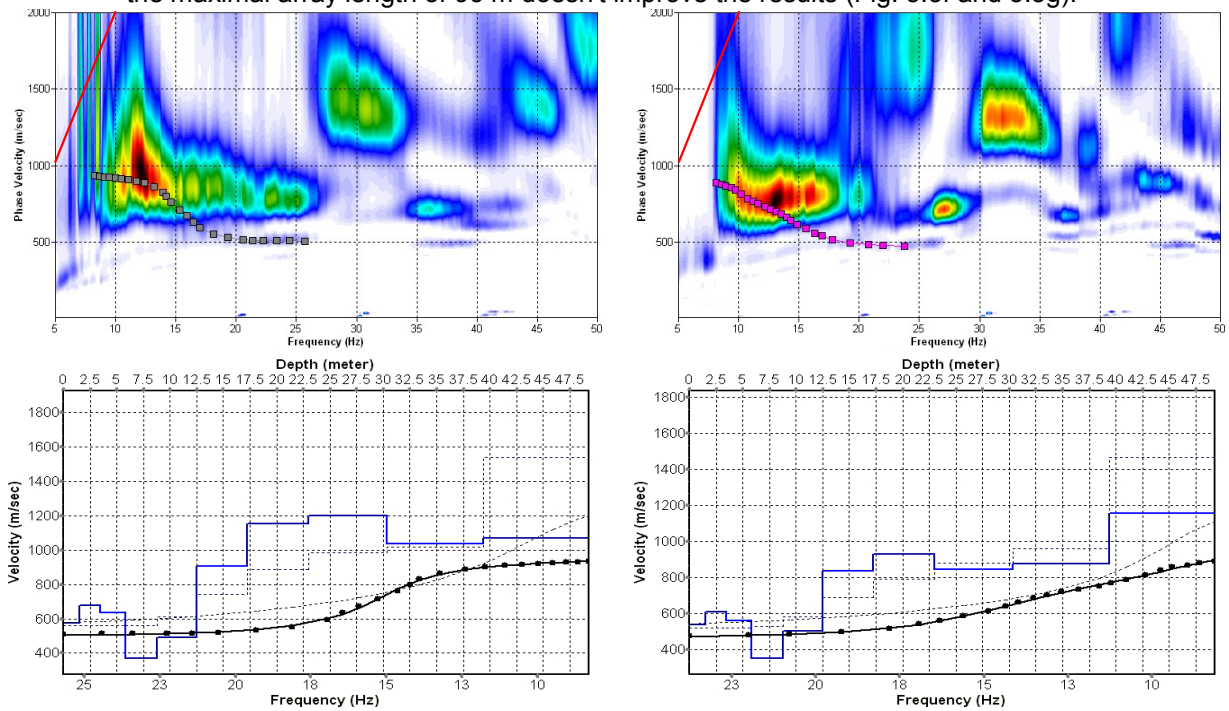

Fig. 3.3f: Top: dispersion images of over-all arrays (10...106 m offset) of line 09SN_19WILA-M1 in PLUS (left) and MINUS (right) direction; dotted fine line: signal-noise ratio for the designated f-v_{ph}-value. Red line: high resolution beam-forming curve for v_{max}.
*Below: The two respective inversion results; **brown**: inversion of dispersion curve; **blue**: 10-layer-model. Horizontal axis: depth, vertical axis: phase velocity resp. v_s.*

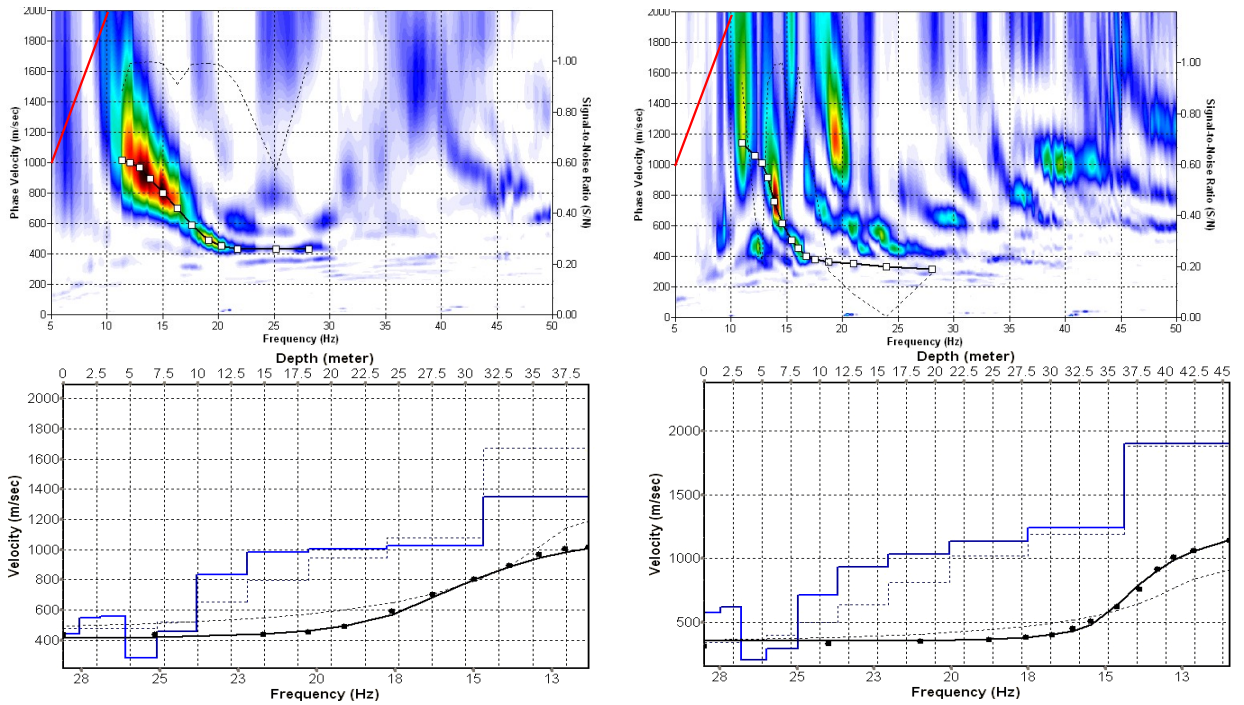

Fig. 3.3g: Top: dispersion images of over-all arrays (10...106 m offset) of line 09SN_19WILA-M2 in PLUS (left) and MINUS (right) direction; dotted fine line: signal-noise ratio for the designated f-v_{ph} – value. Red line: high resolution beam-forming curve for v_{max}.
*Below: The two respective inversion results; **brown**: inversion of dispersion curve; **blue**: 10-layer-model. Horizontal axis: depth, vertical axis: phase velocity resp. v_s.*

3.3.5 Gridding and plotting of 2D v_s-velocity field

By assembling the 1D v_s - depth functions of all stations the final 2D v_s-field is derived using a Kriging gridding procedure as portrayed in Fig. 3.3h and 3.3i below:

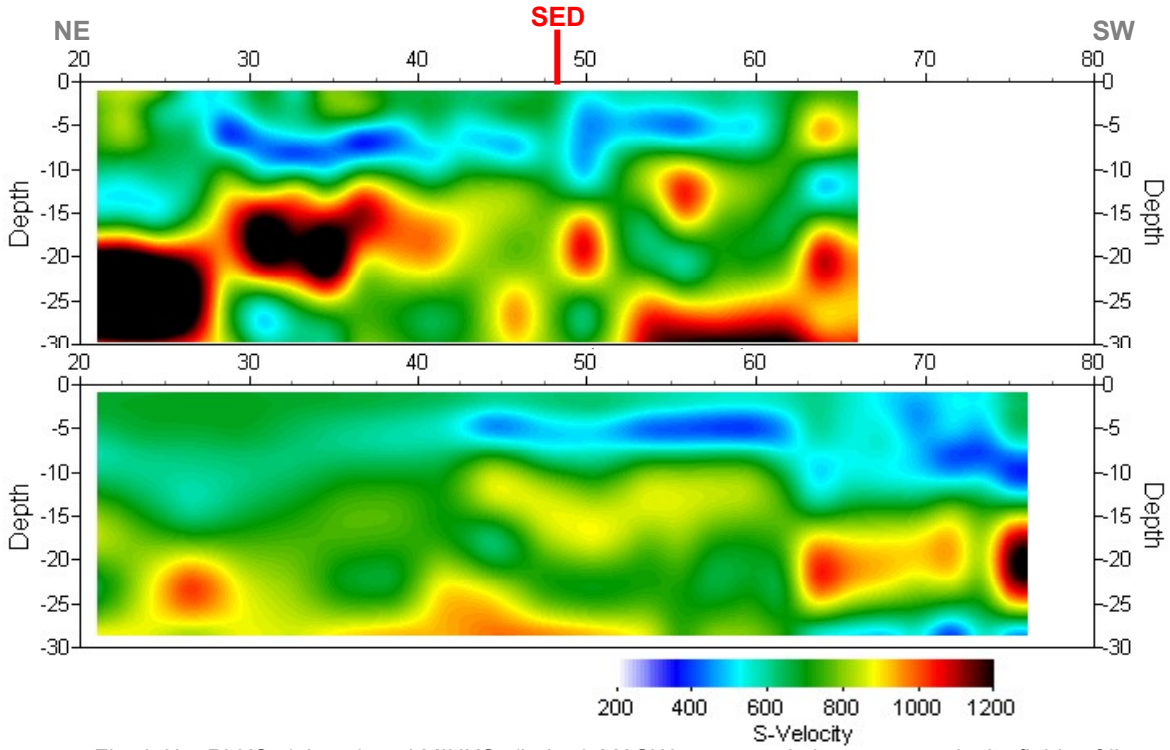

Fig. 3.3h: PLUS- (above) and MINUS- (below)-MASW-processed shear wave velocity fields of line 09SN_19WILA-M1. Station spacing is 1 m.

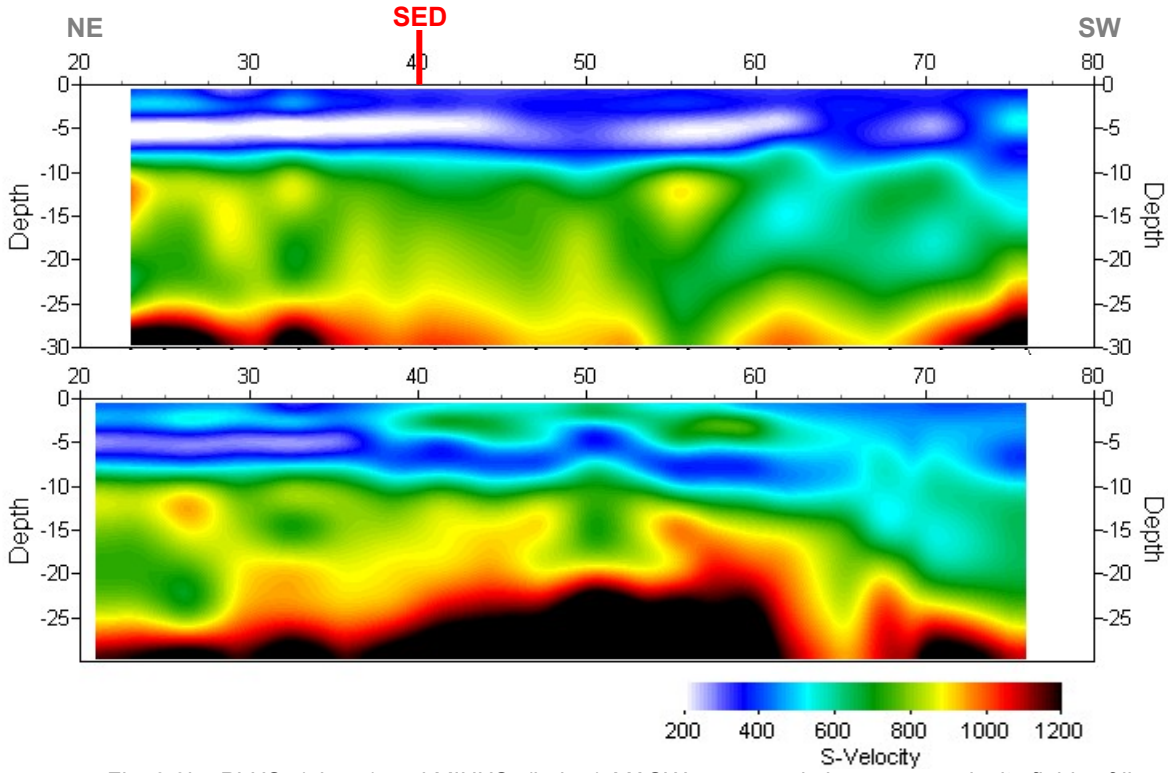

Fig. 3.3i: PLUS- (above) and MINUS- (below)-MASW-processed shear wave velocity fields of line 09SN_19WILA-M2. Station spacing is 1 m.

3.3.6 Calculation of the average shear wave velocity

In order to calculate a representative shear wave velocity-depth function of line 09SN_19WILA-M1 at the SED station, all computed 1D-v_s-depth functions between seismic profile station no. 40 and 60 are averaged (non-weighted mean values). The v_s-depth-function is shown in Tab. 3.3a.

Depth [m]	Vs+ [m/s]	Vs- [m/s]	Vs [m/s]
1.0	661	605	633
2.2	657	607	632
3.7	622	568	595
5.5	572	535	554
7.9	592	559	576
10.8	708	630	669
14.5	835	733	784
19.1	965	817	891
24.8	933	815	874
31.0	934	747	840

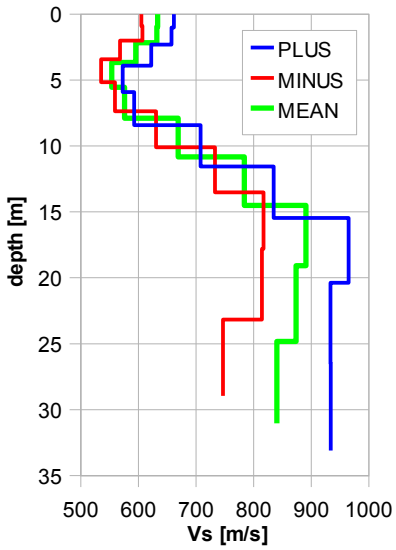

Tab. 3.3a: Averaged vs - depth function of line 09SN_19WILA-M1 at the SED station WILA. Blue line: MASW-'PLUS' processing, red line: MASW-'MINUS' processing; green line: average of PLUS- and MINUS-functions.

In order to calculate an representative shear wave velocity-depth function of line 09SN_19WILA-M2 at the SED station, all computed 1D-v_s-depth functions between seismic profile station no. 40 and 60 are averaged (non-weighted mean values). The resulting v_s-depth-function is shown in Tab. 3.3b.

Depth [m]	Vs+ [m/s]	Vs- [m/s]	Vs [m/s]
0.5	310	353	332
1.2	380	436	408
2.2	409	497	453
4.0	266	410	338
7.0	359	355	357
10.5	683	616	650
14.1	735	735	735
19.0	735	809	772
24.0	808	1000	904
30.0	1106	1322	1214

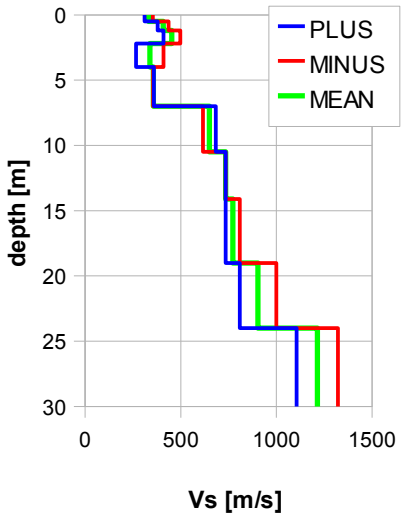

Tab. 3.3b: Averaged v_s - depth function of line 09SN_19WILA-M2 at the SED station WILA. Blue line: MASW-'PLUS' processing, red line: MASW-'MINUS' processing; green line: average of PLUS- and MINUS-functions.

The inversion of the four 100 m-array dispersion curves data (10 to 106 m offset, see Fig. 3.3f and 3.3g) are given in Tab. 3.3c. These values are complemented with the values derived of the 40 m-arrays analyses (Tab. 3.3a and 3.3b).

100 m array								40 m array					
depth	m1+	m1-	m2+	m2-	m1	m2	m	depth	m1	depth	m2	depth	m
1.4	575	538	444	579	557	511	517	1.0	633	0.5	332	0.7	483
3.2	679	609	547	622	644	585	605	2.2	632	1.2	408	1.7	520
5.4	635	559	558	207	597	383	534	3.7	595	2.2	453	2.9	524
8.2	368	351	284	292	360	288	323	5.5	554	4.0	338	4.8	446
11.7	489	503	455	712	496	584	508	7.9	576	7.0	357	7.4	466
16.0	908	834	836	934	871	885	866	10.8	669	10.5	650	10.7	659
21.4	1153	931	981	1032	1042	1007	1018	14.5	784	14.1	735	14.3	759
28.2	1198	844	1002	1136	1021	1069	1028	19.1	891	19.0	772	19.0	831
36.7	1037	878	1027	1241	958	1134	1019	24.8	874	24.0	904	24.4	889
45.8	1068	1154	1347	1903	1111	1625	1299	31.0	840	30.0	1214	30.5	1027

Tab. 3.3c: vs-depth values of the four MASW-derived dispersion curves of both seismic line 09SN_19WILA-M1 and 09SN_19WILA-M2 using 100 m-arrays. The dispersion curves are shown in Fig. 3.3f and Fig 3.3g.

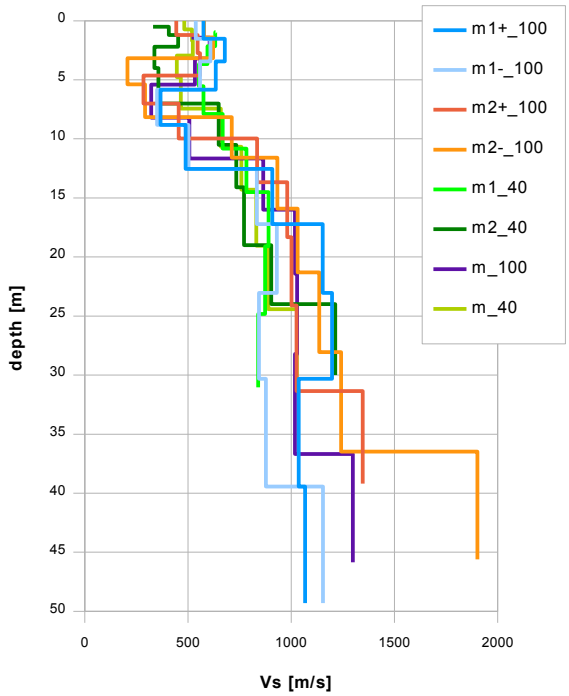

Fig. 3.3j: Comparison of the ensemble of inversion results of both lines 09SN_19WILA-M1 and -M2, either using the 40 m- and the 100 m-arrays.
blue lines: analyses of records of line 09SN_19WILA-M1
red lines: analyses of records of line 09SN_19WILA-M2
violet line: mean of both 100 m-array records analyses in MINUS and PLUS direction.
green lines: v_S-values of analyses of 40 m-array records.

3.3.7 Calculation of the shear wave velocity scalars $v_{s,5}$, $v_{s,10}$, ...

The parameters $v_{s,5}$, $v_{s,10}$, $v_{s,20}$, $v_{s,30}$, $v_{s,40}$, $v_{s,50}$ represent the average shear wave velocities in the depth interval between the surface and the respective depth levels and are determined from the formula

$$v_{s,n} = \frac{\sum_{i=1}^{n} d_i}{\sum_{i=1}^{n} d_i / v_{si}}$$

with:

d_i = thickness of layer i
v_{si} = corresponding shear-wave velocity.

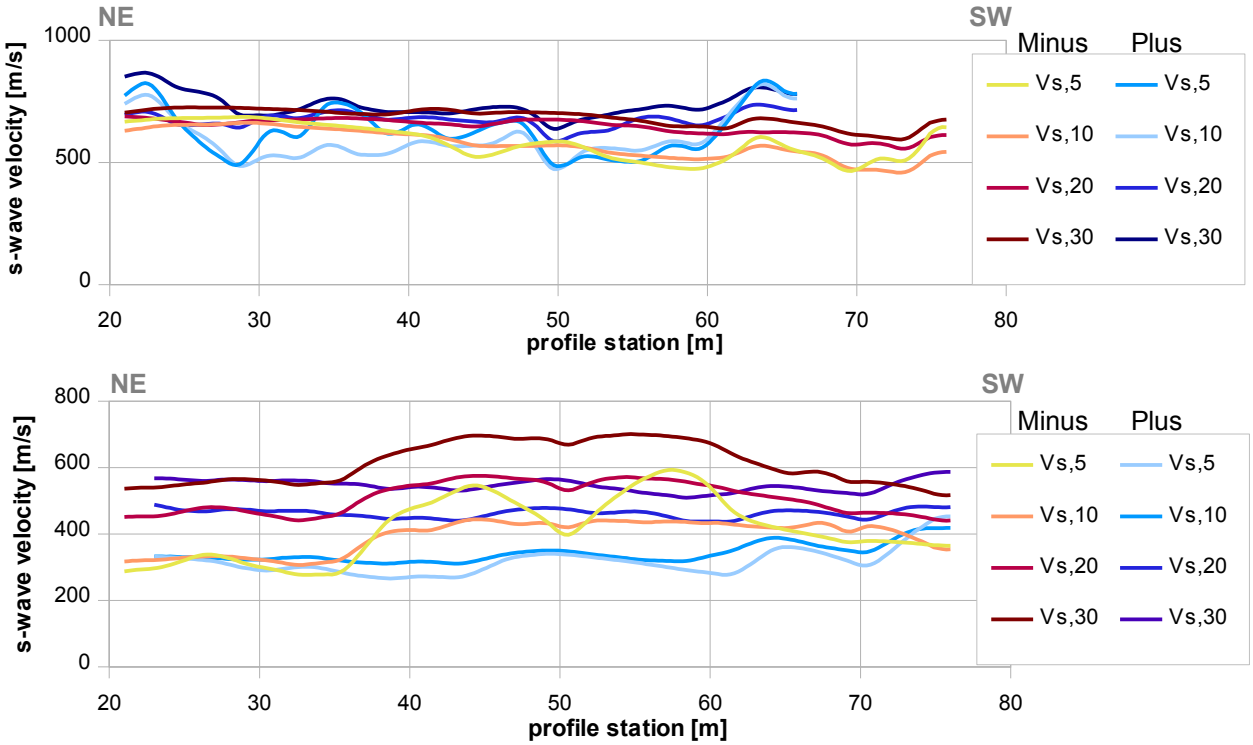

Fig. 3.3k: Graphs of the averaged $v_{s,5}$...-values along the line 09SN_19WILA-M1 (top) and -M2 (bottom) for the PLUS- (blue lines) and MINUS- (red lines) directions.

The average values of the s-wave velocity model $v_{s,5}$, $v_{s,10}$, $v_{s,20}$, $v_{s,30}$, $v_{s,40}$, $v_{s,50}$, $v_{s,100}$ (= average shear wave velocity from the surface to depths of 5 m, …until 100 m) on the line segment nearest to the SED station (Tab. 3.3d) are summarized below:

	Vs,5	Vs,10	Vs,20	Vs,30	Vs,40	Vs,50
MINUS	575	582	661	694	n/a	n/a
PLUS	575	567	658	705	n/a	n/a
MEAN	575	575	659	700	n/a	n/a

	Vs,5	Vs,10	Vs,20	Vs,30	Vs,40	Vs,50
MINUS	322	365	477	513	n/a	n/a
PLUS	329	424	591	709	n/a	n/a
MEAN	326	394	534	611	n/a	n/a

Tab. 3.3d: The average shear wave velocities within the depth intervals from surface down to 5 m, etc.… to 50 m, calculated for the line segment with a subjectively most similar geology to the SED station (station 40 to 60) for line 09SN_19WILA-M1 (above) and -M2 (below).

3.4 Hybrid Seismic Data Processing

3.4.1 p-wave *Reflection* Seismic Processing Sequence

A) Data conditioning

A1 Reformatting and quality verification of field data
A2 Recording geometry assignment
A3 Data editing (suppression of bad / dead traces, etc.)
A4 Preliminary analysis of refraction velocities

B Filtering and deconvolution

B1 Analytical muting of refraction arrivals
B2 Amplitude recovery / amplitude equalization in time and frequency domains
B3 Predictive deconvolution parameter tests / application
B4 Determination of band limiting corner frequencies / application
B5 Optional 2-D filtering

C) Velocity analysis and stack

C1 Common Depth Point (CDP) sort
C2 Semblance velocity analysis using supergathers of 3 - 5 CDP's
C3 Optional dip move-out correction
C4 Normal Move-Out (NMO) correction and application of stretch mute
C5 Band-pass filtering
C6 CDP stack
C7 Optional coherency filtering

D) Time-depth conversion

D1 Optional spiking deconvolution
D2 Band-pass filtering
D3 Depth conversion
D4 Final display of seismic depth section with inversed polarity (non-SEG-convention)

3.4.2 The presentation of reflection seismic data

The data in a reflection seismic section are presented as an assembly of individual seismic signals at regular intervals along a seismic profile. The simplest way of representing the signals are single wiggle lines (first to the left in the illustration below). A more capturing presentation is the variable area form (second to the left). Combining these two modes results in the var-wiggle mode. Another method of data visualization is the variable density mode (second from the right).

The compressional phase of seismic signals is defined in this report as the onset of the positive amplitude excursion in black (Fig. 3.4a). Since the source signal is produced by an explosion or by an impact at the surface, the signal starts off with a compression of the ground particles. Thus the arrivals of reflection events are defined by the compressional phase.

In rare situations of velocity inversions, cases in which formation velocities are lower than in the layers above, polarity reversals of the reflected signals occur. The beginning of the reflection event would then be characterized by a dilatational phase, represented in this report as a negative amplitude excursion, i.e. in white.

The final p-wave seismic depth sections are displayed in Fig. 3.4b and 3.4c, the hybrid sections in Fig. 3.4j and -k further below.

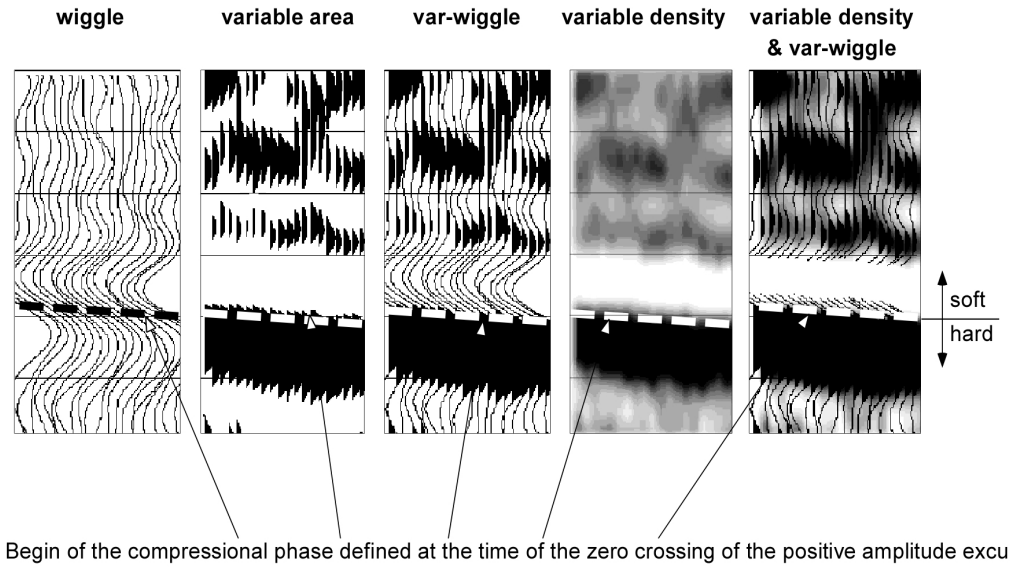

Fig. 3.4a Representation of reflection seismic data and the definition of a reflection event.

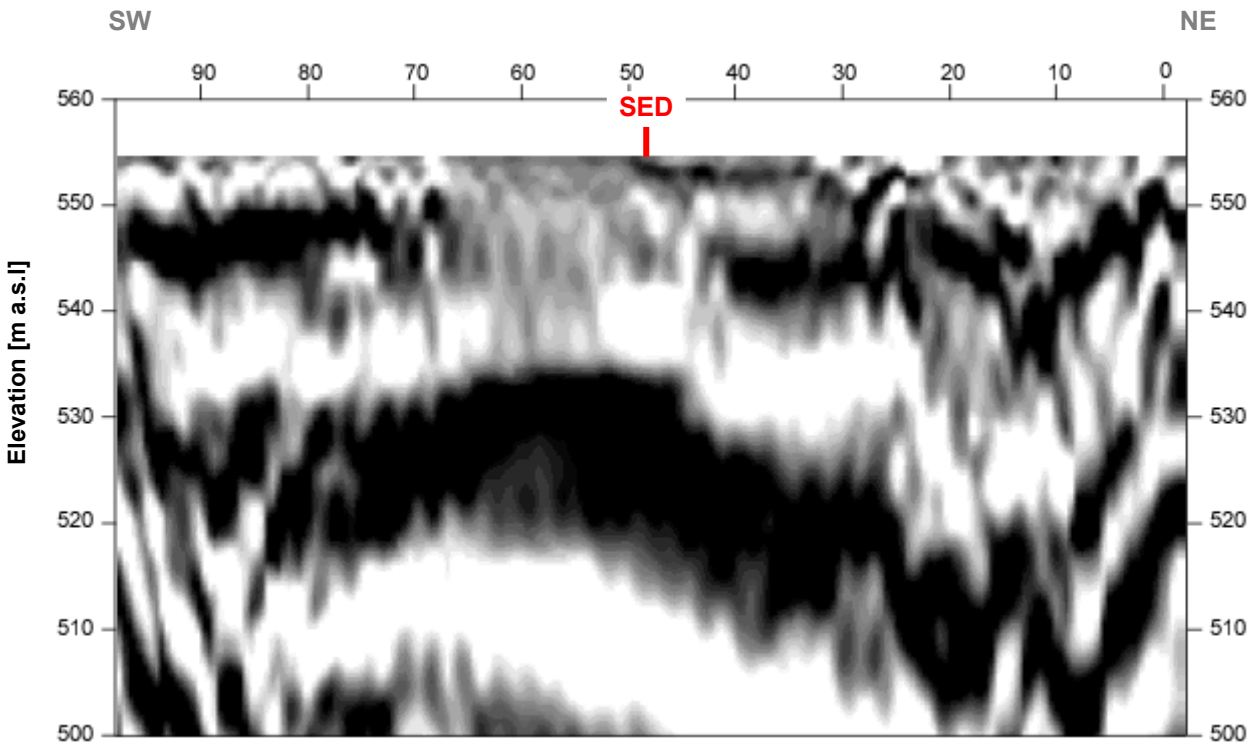

Fig. 3.4b: Seismic depth section of seismic line 09SN_19WILA-P1 with variable density mode presentation. Vertical axis: elevation [m a.s.l.], horizontal axis: profile meter; no vertical exaggeration. The station spacing is 1 m.

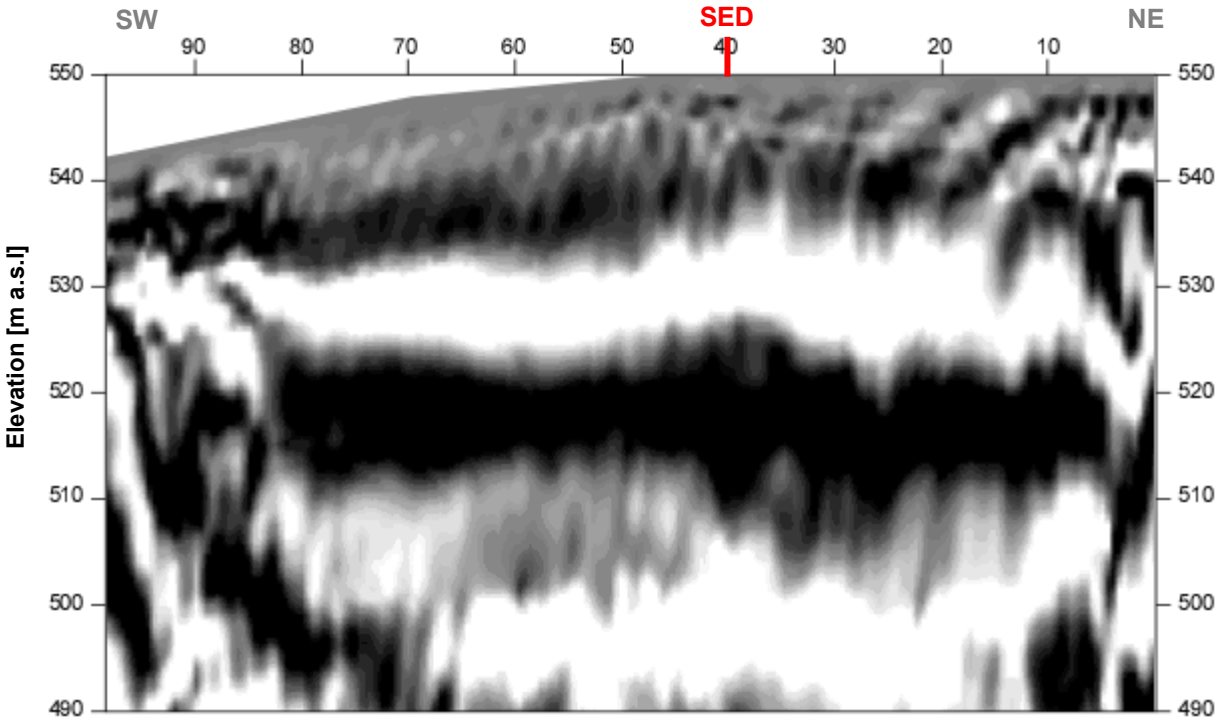

Fig. 3.4c: Seismic depth section of seismic line 09SN_19WILA-P2 with variable density mode presentation. Vertical axis: elevation [m a.s.l.], horizontal axis: profile meter; no vertical exaggeration. The station spacing is 1 m.

3.4.3 p-wave refraction tomography processing

The seismic p-wave refraction processing steps are analogous to those described in paragraph 3.2. For a detailed method statement and a description of the processing steps please refer to the summary report. The Figs. 3.4d to 3.4i and Tab. 3.4a illustrate the intermediate processing steps and the final result.

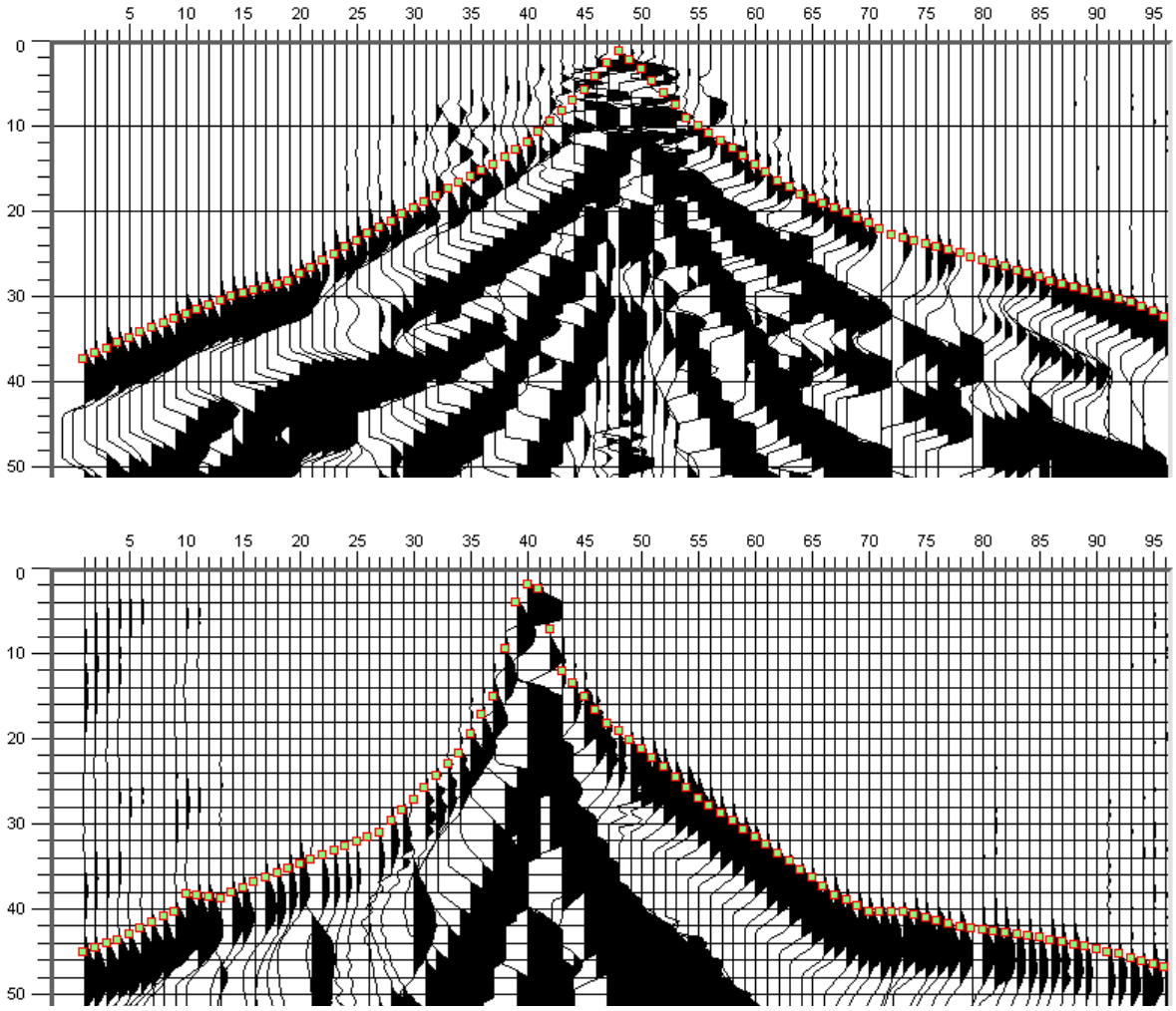

Fig. 3.4d: p-wave records of 09SN_19WILA-P1 (above) and -P2 (below) with positive amplitude excursions in black. Colored dots mark the manually picked first break arrival times. Vertical axis: travel time in ms, horizontal axis: station numbers spaced at 1 m.

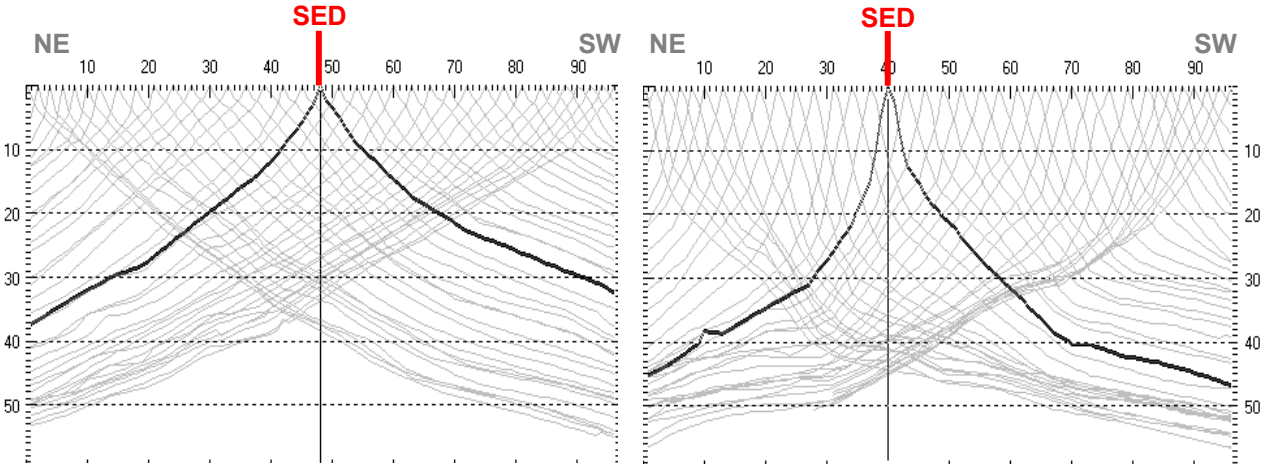

Fig. 3.4e: Travel time curves of p-wave arrival time picks of line 09SN_19WILA-P1 (left) and -P2 (right). Vertical axes: travel time [ms], horizontal axes: station number (= profile meter).

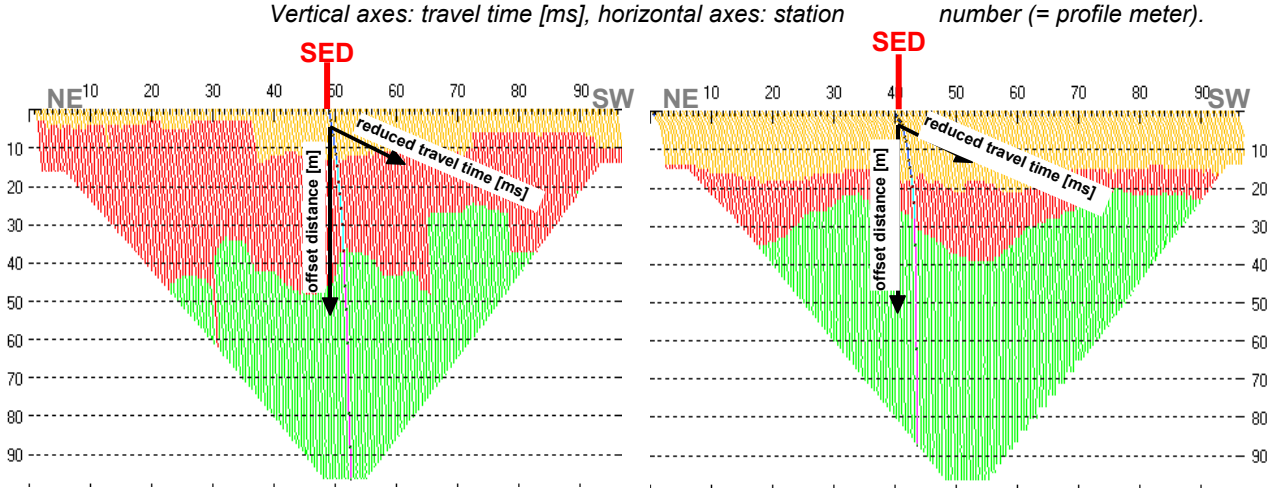

Fig. 3.4f: 3-dimensional distance-travel time diagrams at the mid-points between source points and receiver stations are instrumental when using the analytical CMP derivation of the initial velocity field. The horizontal axes are along the CMP positions and the travel time respectively, the vertical axis denotes the offset distance between source and receiver positions.

Depth [m]	Vp [m/s]
0.2	601
0.5	712
0.8	770
1.4	862
2.0	989
2.9	1115
3.9	1238
5.2	1349
7.1	1565
9.5	1775
12.5	2054
16.4	2412
21.5	2805
28.1	3177
36.7	3737

Depth [m]	Vp [m/s]
0.0	293
0.5	317
0.8	337
1.4	401
2.0	520
2.9	689
3.9	921
5.2	1105
7.1	1269
9.5	1568
12.5	1983
16.4	2456
21.5	3157
28.1	3955
36.7	4524

Tab. 3.4a: Initial 1D p-wave velocity model derived from real data (left: 09SN_19WILA-P1; right: -P2).

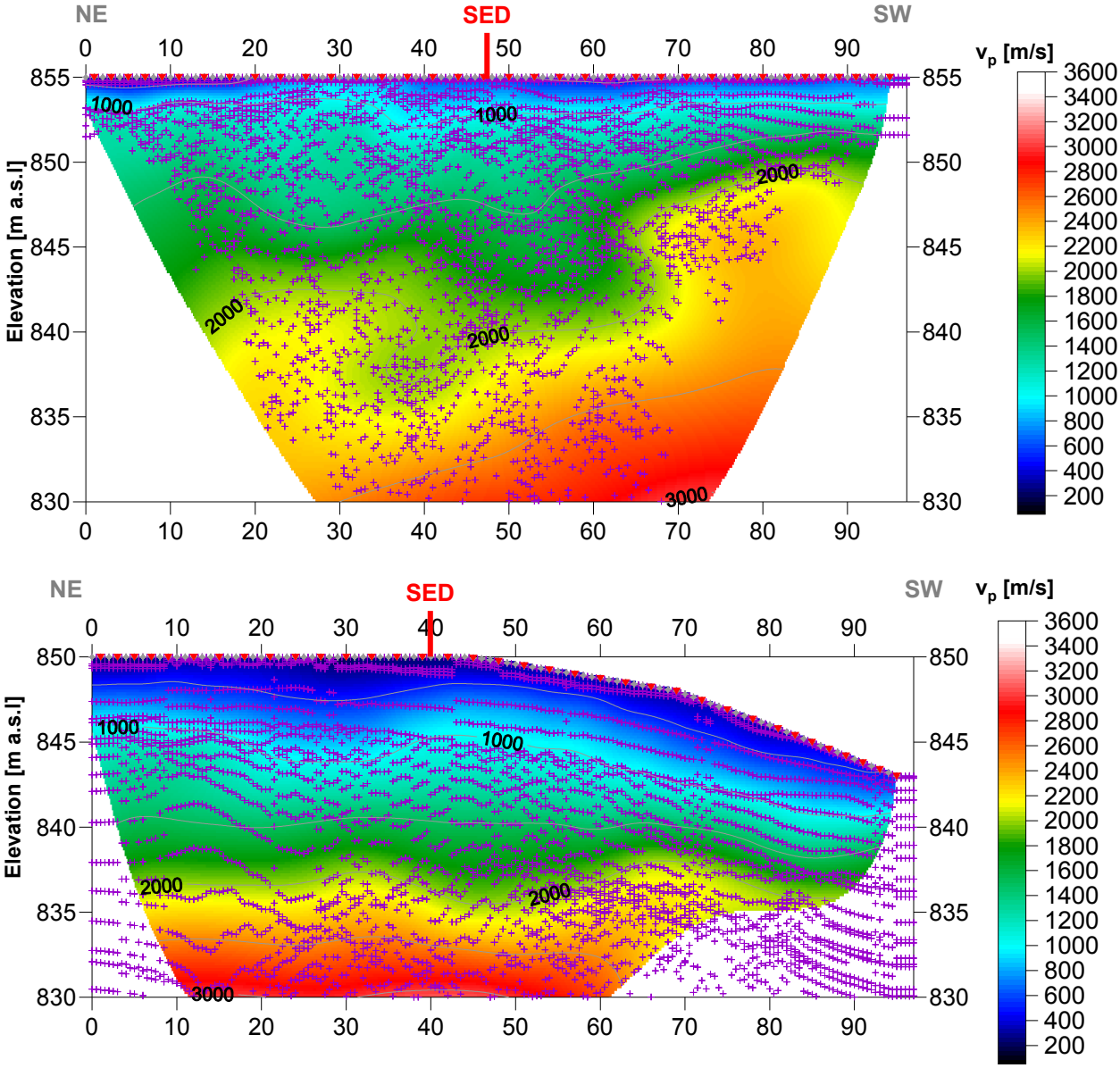

Fig. 3.4g: Compressional wave velocity field image along the seismic profiles 09SN-19WILA-P1 (above) and -P2 (below). Red/white colors indicate solid rock, blue/black colors unconsolidated sediments and soil. Vertical axis: elevation [m a.s.l]; horizontal axis: profile meter; color scale: v_s [m/s]; vertical exaggeration: 2:1; gray squares: receiver stations; red triangles: shot positions; magenta crosses: positions of determined velocity values.

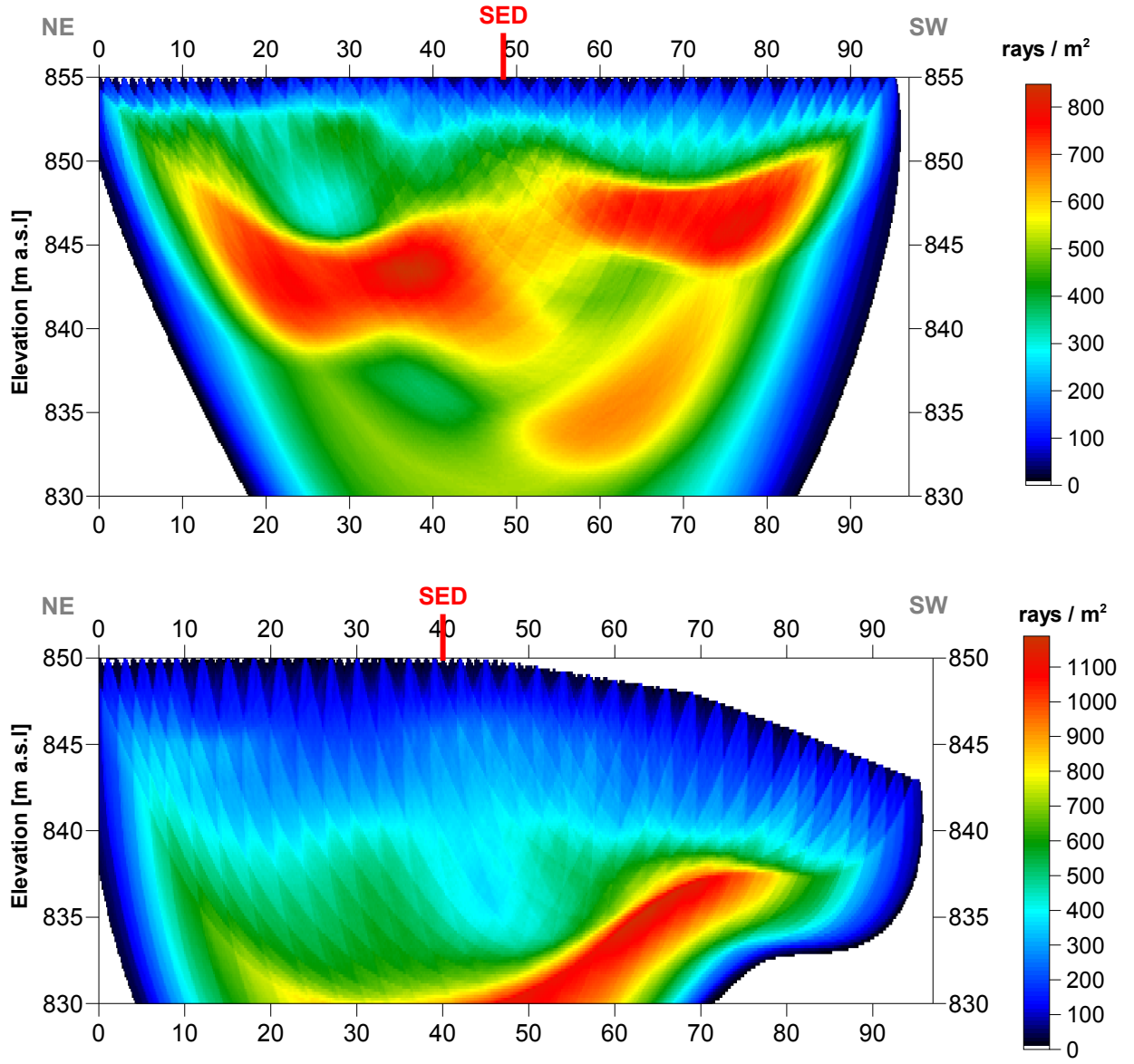

Fig. 3.4h Compressional wave subsurface ray path density along the seismic profiles 09SN_19WILA-P1 (above) and -P2 (below). Red/white colors indicate high velocity contrast between two layers, blue/black colors low coverage areas. Vertical axis: elevation [m a.s.l]; horizontal axis: profile meter; color scale: ray paths per m2; vertical exaggeration: 2:1.

Depth [m]	Vp [m/s]
0.0	565
2.2	995
4.2	1255
6.3	1431
8.3	1582
10.3	1708
12.3	1823
14.4	1953
16.2	2084
18.3	2215
20.3	2374
22.3	2540
24.4	2705
26.4	2878
28.4	3050
30.4	3220

Depth [m]	Vp [m/s]
0.0	298
1.7	564
3.4	861
5.1	1037
6.8	1184
8.5	1380
10.1	1607
11.8	1804
13.5	1989
15.2	2203
16.7	2484
18.4	2778
20.1	3061
21.8	3351
23.5	3603
25.2	3775

Tab. 3.4b: Final 1D p-wave velocity model derived from real data at positions most similar to the geological setting at SED station between profile meters 40 and 60 at both lines 09SN_19WILA-P1 (left) and -P2 (right).

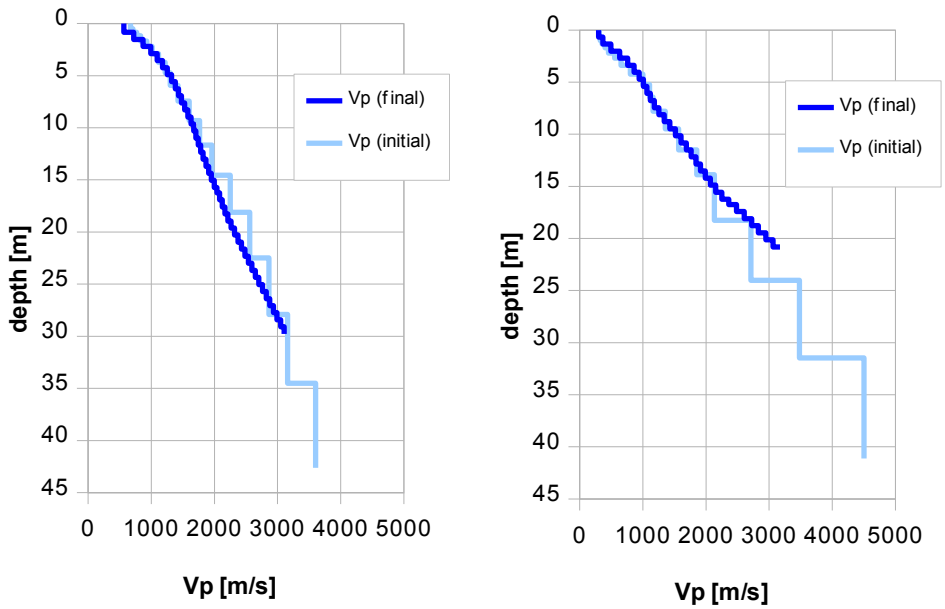

Fig. 3.4i: Final 1D p-wave velocity model derived from real data at a position most similar to the geological setting at SED station between profile meters 40 and 60 at both lines 09SN_19WILA-P1 (left) and -P2 (right).

3.4.4 Representation of the hybrid seismic section

The hybrid seismic section is the reflection seismic section with the superimposed p-wave velocity field. It portrays the geological structures and the p-wave velocity field, the latter being indicative for the rock / soil rigidity. The uninterpreted hybrid seismic section is portrayed in Fig. 3.4j and 3.4k below.

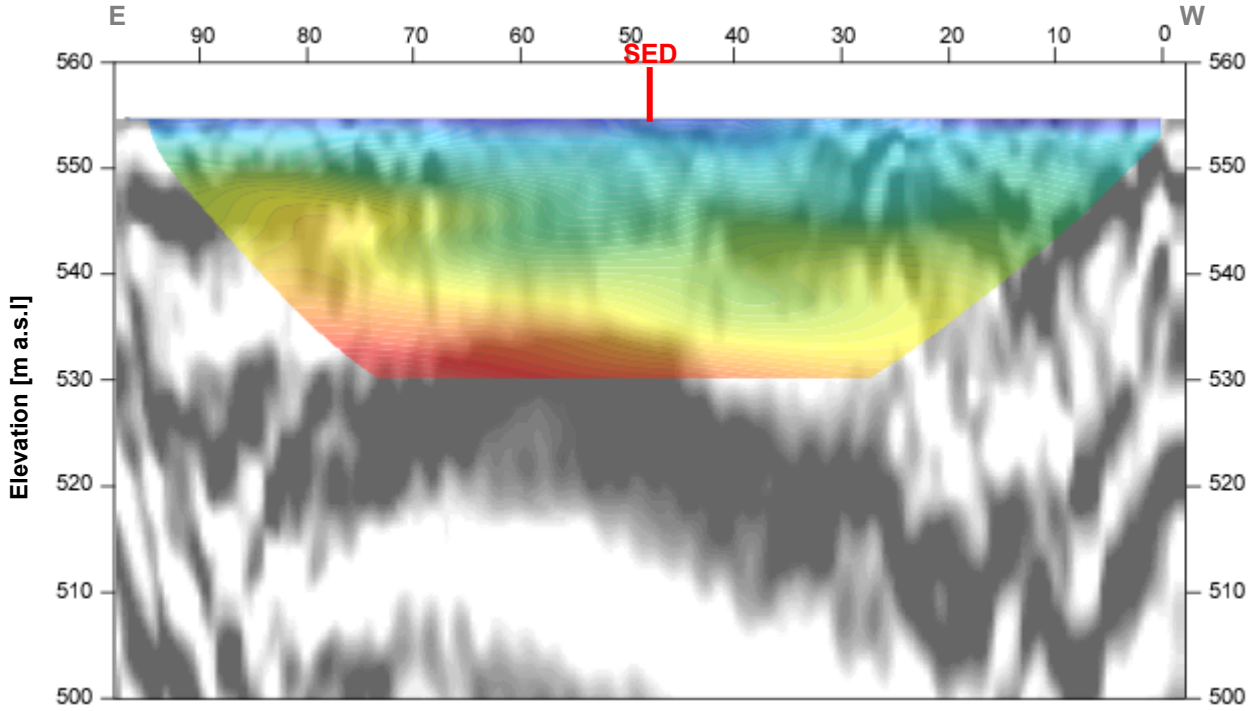

Fig. 3.4j Uninterpreted hybrid seismic section 09SN_19WILA-P1: superimposed onto the seismic reflection section is the color encoded p-velocity field derived by refraction tomography (no vertical exaggeration).

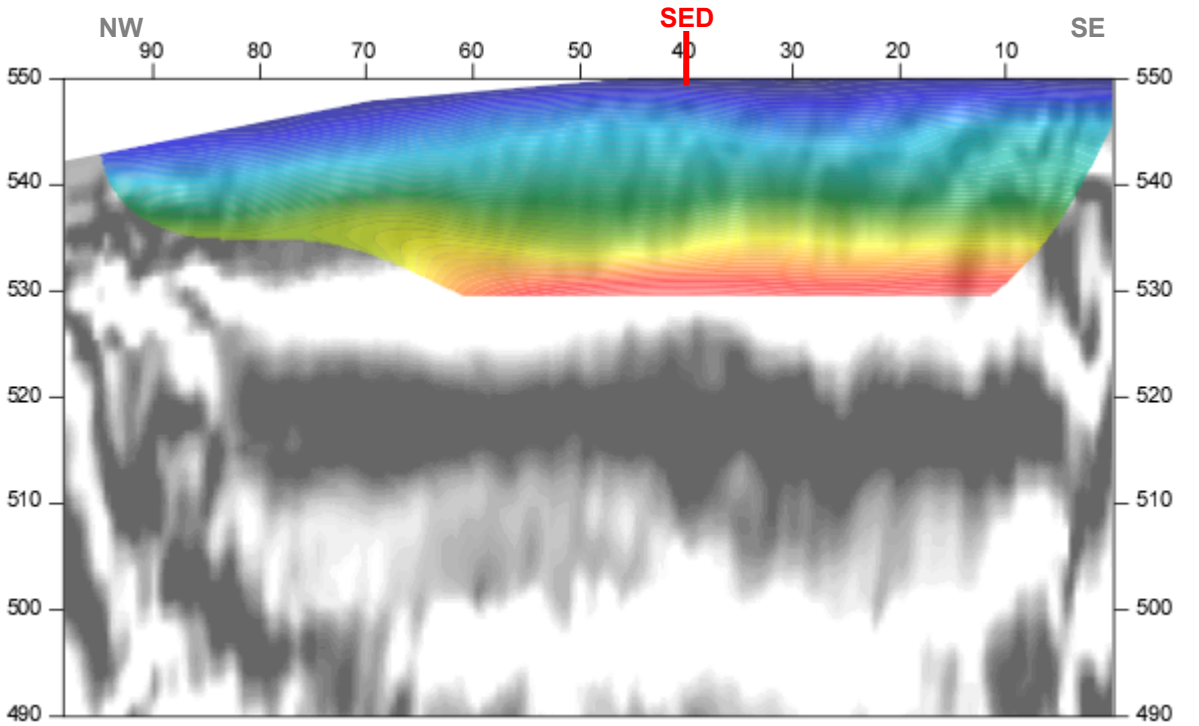

Fig. 3.4k Uninterpreted hybrid seismic section 09SN_18WILA-P2: superimposed onto the seismic reflection section is the color encoded p-velocity field derived by refraction tomography (no vertical exaggeration).

4 DISCUSSION OF THE RESULTS

4.1 Summary and Validation of the Results

Compressional and shear wave velocity data from refraction seismic surveys both p-wave and s-wave and also the MASW survey data of profiles 09SN_19WILA-1 and 09SN_19WILA-2 are shown in Tab. 4.1 for the uppermost 30 m. The calculated shear wave velocity $v_{s(calc)}$ in Tab. 4.1 is derived by using a theoretical v_p/v_s-ratio of $\sqrt{3}$.

Depth	Vp1	Vp2	Vs1	Vs1	Vs2	Vs2	Vs1	Vs2
	meas	meas	meas	calc	meas	calc	MASW	MASW
0	565	298		326	163	172		332
1	724	367	931	418	187	212	633	408
2	872	494	790	504	228	285	632	453
3	1095	759	833	632	304	438		
4	1178	861	938	680	345	497	595	338
5	1323	1008	1067	764	380	582		
6	1381	1064	1213	797	420	614	554	
7	1480	1184	1354	854	446	683		357
8	1530	1256	1477	883	484	725	576	
9	1582	1425	1627	913	485	823		
10	1672	1517	1794	965	474	876		650
11	1708	1691	1922	986	452	976	669	
12	1781	1767	2009	1028	440	1020		
13	1823	1915		1052	459	1105		
14	1910	1989	2057	1103	488	1149		735
15	1953	2156	2054	1128	542	1245	784	
16	2041	2253	2008	1178	572	1301		
17	2126	2484	2029	1228	640	1434		
18	2169	2607	2158	1252	670	1505		
19	2265	2832	2289	1308	699	1635	891	772
20	2319	2947	2333	1339	771	1702		
21	2374	3173	2295	1371	816	1832		
22	2485	3293	2204	1435	873	1901		
23	2540	3504	2070	1466	879	2023		
24	2649	3603	1930	1530	877	2080		904
25	2705		1870	1562	881		874	
26	2821		1924	1628	896			
27	2878		2056	1662	915			
28	2993		2230	1728	938			
29	3050		2379	1761	963			
30	3163		2492	1826	1015			1214
31	3220		2585	1859	1041		840	
32	3329		2684	1922				

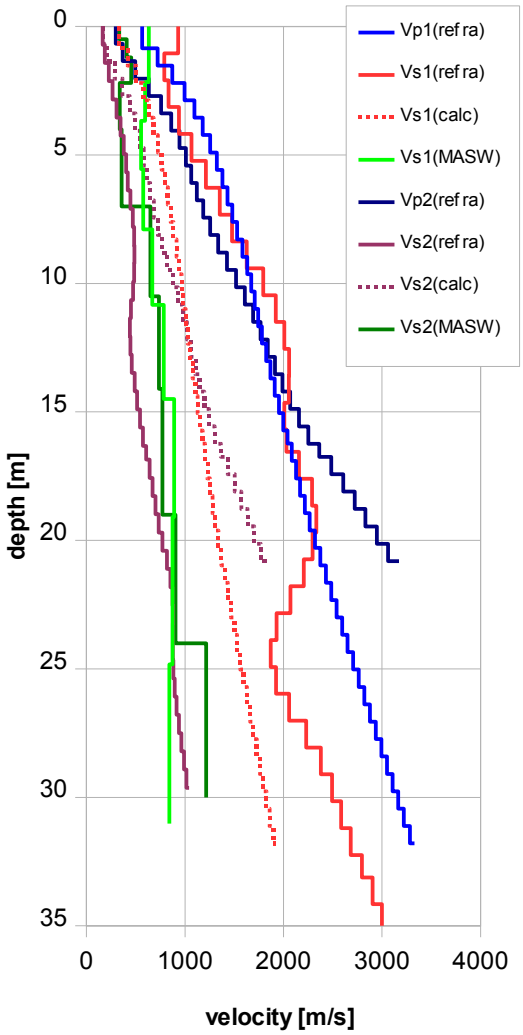

Tab. 4.1: Shear and compressional wave velocity model determined at the SED station WILA.

Fig. 4.1: Graphic display of shear (continuous lines) and compressional (dotted lines) wave velocities determined at the SED station. In green colors values of line 09SN_19WILA-1 and in blue values of line 09SN_19WILA-2. at the SED station.

4.2 Validation of the methods and their results

Due to methodological differences, v_s velocities derived by MASW analysis and by the refraction tomography technique may differ considerably. This is because MASW analysis cannot image small rock/soil inhomogeneities as a dispersion image with an array length of i.e. 40-m only yields one single v_s-value at each depth. On the other hand, refraction diving wave tomography results produce v_s-sections with a high lateral resolution, but fail to provide information at greater depths.

4.3 Error Estimates

The error estimates given in Tab. 4.3 below are relevant only in the context of this survey.

Surveying method	Type of result	Error estimate
v_s – refraction tomography, line S1	v_s – velocity field image	100%*
v_s – refraction tomography, line S2	v_s – velocity field image	15%
MASW only "+" or only "-" values*	v_s – velocity field image	15%
MASW (mean of "+" & "-" values)*	v_s – velocity field image	8%
v_p – refraction tomography	v_p – velocity field image	8%
Reflection seismic surveying	Image of subsurface structures	n.a.

* *too high v_s – refraction tomographic values on line S1 cause in lack of good data due to asphalt seal.*

Tab. 4.3 Error estimates for the methods applied. Note that higher error estimates are to be taken into account with increasing depths.

The above error estimates are of a qualitative character only. Shear wave refraction tomography on line 09SN_19WILA-S1 has objectively too high values. Due to deficient bonding between source (shear wave beam) and asphalt seal, the . In particular the topography variations on line 09SN_19WILA-1 have a certain impact on the quality of dispersion images. Nevertheless, all velocity data coincide well, independently of the methodological differences.

At the SED station WILA (Turbenthal ZH), the refraction velocity images both from shear and compressional wave analysis show coincident structures. The MASW figures are in the same range as the values obtained from the shear wave diving wave refraction tomography survey (09SN_19WILA-S2).

4.4 The Geophysical Interpretation

The most conclusive information about the subsurface structures is provided by the results of the hybrid seismic section (v_p-refraction tomography profiling and reflection seismic section) and confirmed by the evaluation results of the v_s-refraction tomography data (only line 09SN_19WILA-2).

As can be seen from the v_s and v_p refraction tomography sections in Fig. 3.4g/h, the topography of the bedrock surface is imaged well. The geological interpretation of the seismic events is shown in Fig. 4.2a. The solid rock surface shows an escarpment at station 60 of about 3 to 5 m. To the NW, the layering in the molasse dips strongly to NW, in contrast to the SE part, where no clear dipping is observed.

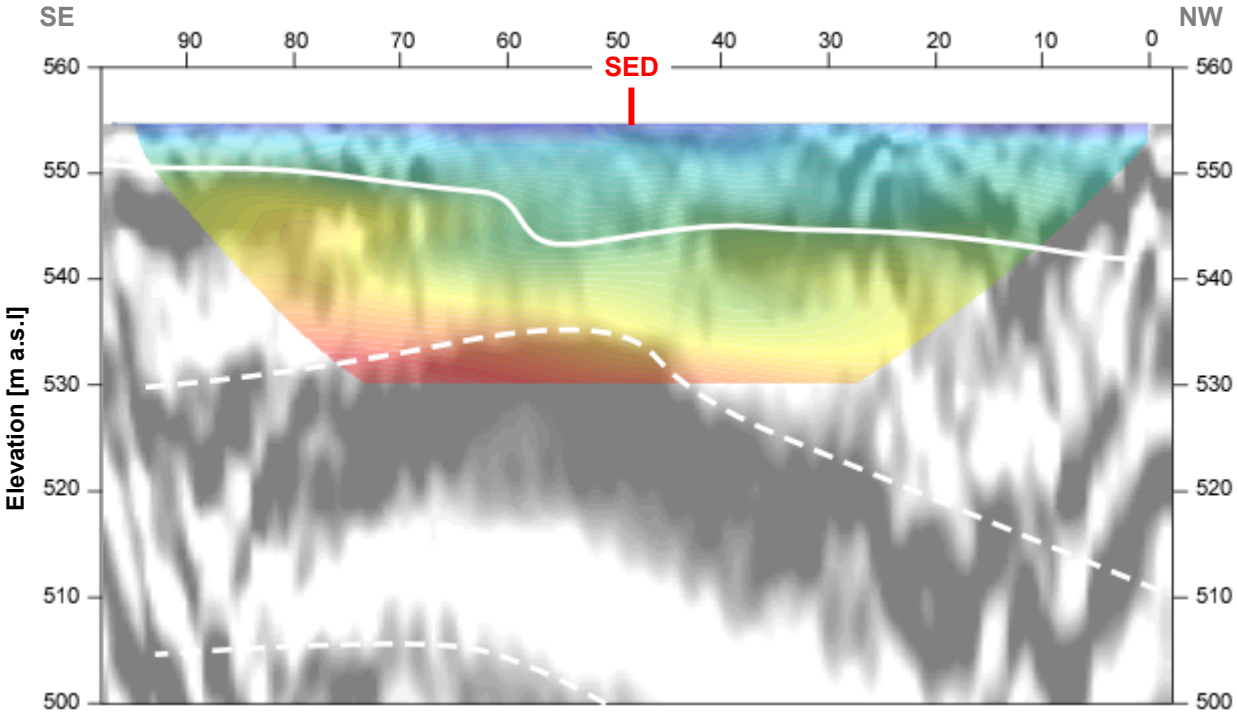

Fig. 4.2a Geophysical interpretation of the hybrid seismic section 09SN_19WILA-P1. White lines denote layer boundaries, continuous line the bedrock surface.

The geological interpretation of the seismic events of line 09SN_19WILA-2 is shown in Fig. 4.2b. The topography of the hard bedrock is slightly horizontal in a depth of 4 m (SW) to 13 m (NW), also the observed layering in the rock below.

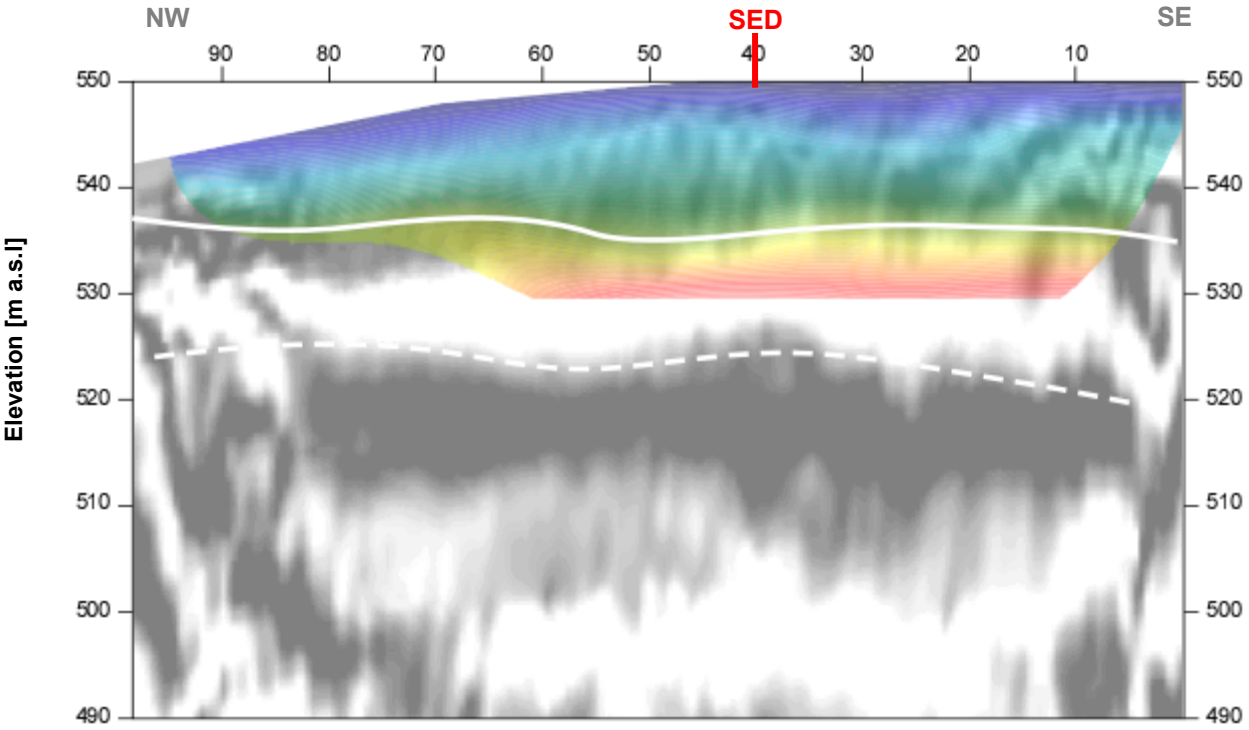

Fig. 4.2b Geophysical interpretation of the hybrid seismic section 09SN_19WILA-P2. White lines denote layer boundaries, the continuous one marks the bedrock surface.

5 SUMMARY AND CONCLUSIONS

- In April 2009 a combined seismic s- and p-wave survey was carried out at the SED earthquake monitoring station WILA near Turbenthal ZH.
- The shear wave data have been evaluated by conventional diving wave refraction tomography techniques in order to derive the s-wave velocity field along the seismic line. Due to poor coupling of the source to the ground (sealing asphalt), the results of line 1 are to be rated as insufficient.
- The p-wave data have been processed
  - firstly to derive a 2D s-wave velocity field by using the MASW (**M**ultichannel **A**nalysis of **S**urface **W**aves) technique;
  - and secondly, according to the hybrid seismic data processing scheme for representing the subsurface structures in a combined reflection seismic section with the superimposed p-wave velocity field.
- The shear wave velocity range determined by the MASW method in the uppermost 30 meters spans from values of 554 to 840 m/s on sealed ground and from 310 m/s to 1322 m/s on the dirt road.
- The scalar values derived by the MASW survey at the SED station (seismic line 09SN_19WILA-M1, profile station 50 resp. seismic line 09SN_19WILA-M2, profile station 50) are the following:

line 1			line 2		
$v_{s,5}$	=	575 m/s	$v_{s,5}$	=	363 m/s
$v_{s,10}$	=	575 m/s	$v_{s,10}$	=	362 m/s
$v_{s,20}$	=	659 m/s	$v_{s,20}$	=	487 m/s
$v_{s,30}$	=	700 m/s	$v_{s,30}$	=	579 m/s
$v_{s,40}$	=	n/a	$v_{s,40}$	=	n/a

- The maximum refraction shear wave velocity derived from line 09SN_19WILA-S2 is 1015 m/s at a depth of 30 m.
- The maximum p-wave velocity determined is 3603 m/s at a depth of 24 m.
- The geophysical interpretation of the subsurface structures in this report are to be validated and incorporated into a comprehensive appraisal by a geologist familiar with the local geological setting.

Schwerzenbach, 12th June 2009

Walter Frei
dipl. Natw. ETH
managing director

Lorenz Keller
dipl. Natw. ETH
project manager